Acta Astronautica 209 (2023) 48–66

Contents lists available at ScienceDirect

Acta Astronautica

journal homepage: www.elsevier.com/locate/actaastro

Review article

# Oxygen–methane rocket thrust chambers: Review of heat transfer experimental studies

Marco Pizzarelli [a,*], Francesco Battista [b]

[a] ASI - Italian Space Agency, Rome, Italy
[b] CIRA - Italian Aerospace Research Centre, Capua (CE), Italy

ARTICLE INFO

*Keywords:*
Rocket thrust chambers
Oxygen–methane propulsion
Heat transfer
Experimental studies
Fluid Dynamics

ABSTRACT

Nowadays oxygen–methane propulsion is considered of great potential for the next generation of operational rockets. In the development of a new liquid rocket engine with high-performance, an essential assessment is the thermal behavior of the thrust chamber. In fact, the flow of combustion gas inside the thrust chamber induces a level of wall temperature and heat flux such as to limit the life of this component. Furthermore, the heat transfer within the thrust chamber directly impacts the performance of the rocket engine. In the present study, a thorough survey of the open literature concerning the experimental activities focused on the heat transfer within oxygen–methane thrust chambers is carried out in order to identify the most consolidated results and the aspects that would require further investigations. The results are divided into three main categories: hot-gas side heat transfer; coolant heat transfer and wall compatibility; thrust chamber life.

## 1. Introduction

The hot-gas generated and accelerated in a liquid bi-propellant rocket engine thrust chamber creates an extremely harsh environment that represents one of the major design constraints for such component, especially when the engine specific impulse is maximized. In fact, the temperature $T_0$ of the hot-gas in the initial part of the thrust chamber, often referred to as combustion chamber, is "high" (up to about 3500 K) because of the increase of the specific impulse with $T_0$. Also the pressure in the combustion chamber, $p_0$, is "high" (up to about 300 bar) mainly because, for a given engine thrust and nozzle exit area, the larger $p_0$ the larger the specific impulse. Ultimately, with such temperature and pressure requirements, rocket engine cooling is necessary to keep the walls at a sufficiently low temperature, so that the wall material is strong enough to withstand the stresses imposed by the thermal gradients, fluid pressure, and other loads like engine thrust and vibrations. Suitable cooling is achieved by flowing one of the two propellants into a number of cooling channels that constitute the thrust chamber structure. Often the fuel is used for this purpose and not the oxidizer, in order to limit wall oxidation problems [1,2]. The term regenerative cooling is used because the coolant is not wasted as it is used as a propellant. When the thrust chamber is realized with conventional manufacturing, the channels are milled from a forged bulk part and the outer wall, which is generally composed of a different material, is joined afterward. Differently, in case of additive manufacturing the thrust chamber is generally made in a single build process and thus it is made of a single material, although an external high-mechanical-strength material can also be deposited [3]. A scheme of a typical conventionally-manufactured, regeneratively-cooled thrust chamber is shown in Fig. 1.

The life of a thrust chamber is mainly limited by the level of wall temperature and heat flux reached in the most thermally solicited parts, that are the throat and near injection regions. Consequently, the design of a thrust chamber is mainly a thermo-mechanical problem that can be assessed only with a proper characterization of the hot-gas side and coolant side heat transfer as well as specific related issues like the coolant compatibility with the wall material. Furthermore, the heat transfer within the thrust chamber directly affects rocket engine performance as it impacts the amount of coolant mass flow rate to be pumped into the cooling circuit and the coolant pressure drop, as well as the heat absorbed by the coolant which can be used as an energy source for the engine.

In view of the widespread interest in the oxygen–methane propulsion, which is expected to be used on the next generation of many operational rockets, a thorough survey of the open literature concerning the experimental activities focused on the heat transfer within oxygen–methane thrust chambers is carried out in order to draw conclusions on the better understood aspects and those that need further investigation. After presenting the main aspects that drive rocket designers to select oxygen–methane propulsion (Section 2), the most

* Corresponding author.
*E-mail address:* marco.pizzarelli@asi.it (M. Pizzarelli).

https://doi.org/10.1016/j.actaastro.2023.04.028
Received 1 January 2023; Received in revised form 7 March 2023; Accepted 15 April 2023
Available online 21 April 2023

**Nomenclature**

| | |
|---|---|
| $c_p$ | specific heat at constant pressure, [J/(kg K)] |
| $D$ | diameter, [m] |
| $f$ | friction factor, [-] |
| $k$ | thermal conductivity, [W/(m K)] |
| $\dot{m}$ | mass flow rate, [kg/s] |
| $Nu$ | Nusselt number, [-] |
| $p_0$ | hot-gas pressure in the combustion chamber, [Pa] |
| $\Delta p$ | pressure drop, [Pa] |
| $Pr$ | Prandtl number, [-] |
| $Re$ | Reynolds number, [-] |
| $T$ | temperature, [K] |
| $T_0$ | hot-gas temperature in the combustion chamber, [K] |
| $u$ | velocity, [m/s] |
| $x$ | axial abscissa, [m] |

**Greek**

| | |
|---|---|
| $\varepsilon$ | equivalent sand grain roughness, [m] |
| $\mu$ | dynamic viscosity, [Pa s] |
| $\rho$ | density, [kg/m$^3$] |

**Subscripts**

| | |
|---|---|
| $b$ | fluid property at bulk temperature |
| $w$ | fluid property at wall temperature |
| $sat$ | saturation |

relevant experimental studies are described and discussed. In particular, the hot-gas side heat transfer studies are presented in Section 3, the coolant heat transfer and wall compatibility studies are presented in Section 4, and, finally, the thrust chamber life experiments are presented in Section 5.

## 2. Oxygen–methane propulsion: why?

Oxygen–methane has been considered a promising propellant combination since the early development of rocket propulsion, although nowadays the most widely used propellant combinations are oxygen–hydrogen, oxygen–kerosene, and hypergolic combinations like nitrogen tetroxide-hydrazine (the latter, in the form of pure hydrazine, or mono-methyl hydrazine, or unsymmetrical dimethylhydrazine, or their mixtures) [1]. It is worth noticing that the latter combination ignites spontaneously and is storable (i.e., liquid at room temperature) while all the others need an ignition device and are cryogenic (i.e., at least one of the two propellants is liquid only below the room temperature).

The main advantages in using methane as a fuel over hydrogen are related to its higher liquid storage temperature and density. Storage temperature of liquid methane is much warmer than hydrogen (about 110 K versus 20 K, respectively) and is closer to the storage temperature of oxygen (about 90 K). This reduces handling efforts, simplifies the thermal management of the vehicle storage system, and reduces the heat-transfer between the propellant tanks. Moreover, the oxygen–methane propellant combination can be considered "space-storable", as its liquid storability in space is much easier than when using hydrogen thanks to the lower boil-off losses. While oxygen–methane propulsion provides a much lower specific impulse with respect to oxygen–hydrogen propulsion (up to 370 s versus up to 470 s, respectively), liquid methane is 6 times denser than liquid hydrogen (about 420 kg/m$^3$ versus about 70 kg/m$^3$), leading to better vehicle design because of the reduced weight and dimension of the tank, as well as aerodynamic drag losses. Moreover, methane, thanks to the larger size of its molecule, has fewer leakage problems than hydrogen. Concerning the thrust chamber thermo-mechanical design, methane used as coolant reduces the temperature difference within the structure, resulting in a less dramatic thermal strain compared to oxygen–hydrogen engines.

The main advantages in using methane as a fuel over kerosene are higher specific impulse (up to 370 s versus up to 350 s, respectively), better cooling performances, and, because of the lower carbon content of the methane molecule, less carbon deposition in the form of soot in the exhaust products or coke when used as coolant. However, methane is about 2 times less dense than kerosene (about 420 kg/m$^3$ versus about 800 kg/m$^3$), resulting in larger tanks. Moreover, in case of fuel-cooled thrust chambers, as kerosene is storable while methane is stored at about 110 K, the temperature difference within the structure of an oxygen–methane thrust chamber is substantially higher than in a oxygen–kerosene thrust chamber, resulting in higher thermal strain.

With respect to hypergolic propellants, the advantages of oxygen–methane propellant combination are low toxicity and improved specific impulse (up to 370 s versus up to 340 s, respectively). However, oxygen–methane propulsion requires an ignition system, increasing the system complexity.

When considering oxygen–methane propulsion, it is worth considering that natural gas, because of the high methane content (often over 90%) is a possible cheaper alternative to pure methane. However, even if the other components of natural gas, mainly ethane and propane, have a limited negative impact on the performance in terms of specific impulse, it is necessary to minimize the presence of undesired species, like the corrosive sulfur compounds.

Historically, NASA considered oxygen–methane propulsion in late 1970s through the 1980s as a credible candidate for booster engines because of its compromise between the density of oxygen–kerosene and the performance of oxygen–hydrogen [4,5]. Because of the envisioned booster engine application, the combustion chamber conditions were at relatively high chamber pressures (at least larger than 100 bar). Starting from the 2000s, NASA renewed the interest on this propellant combination for in-space rather than booster applications [6–9]. Oxygen–methane propulsion for planetary landing/ascending or orbit maneuvers would replace the toxic hypergolic propellants (like nitrogen tetroxide-hydrazine) that are typically used for such applications. Besides the higher specific impulse, the advantages over hypergolic propellants for in-space propulsion are the safer environment for the ground crews and astronauts when manipulating oxygen and methane, the possibility to produce these propellants in situ, thus reducing the need to carry them to extraterrestrial surfaces, and the ability to use common tanks for other subsystems (e.g., oxygen for life-support systems, methane for solid-oxide fuel cell power systems). To be noted that even if an ignition system is required because oxygen–methane is not a hypergolic combination, the relatively high vapor pressure simplify the ignition in vacuum. For in-space application, the desired combustion chamber conditions are at relatively low chamber pressures (generally not larger than 20 bar).

More recently, driven by the need to lower operational costs, oxygen–methane fed engines for booster and sustainer applications are at an advanced stage of development all around the world (mainly: US, Europe, China, and Japan) and will soon be employed on the next generation of rockets (e.g., [10–17]). The main cost reduction margins are attributed to the trade-off between liquid propellant density and specific impulse that allows relatively compact stage design, to the similar and modest temperature of liquid oxygen and methane that simplifies tank architecture due to reduced heat transfer between tanks and with the external environment, to the very low formation of coke and soot that facilitates the refurbishment of reusable stages between launches, to the low flammability and toxicity that makes ground logistics operations safer and less expensive, and to the relatively low cost of propellants (especially in the case of natural gas).

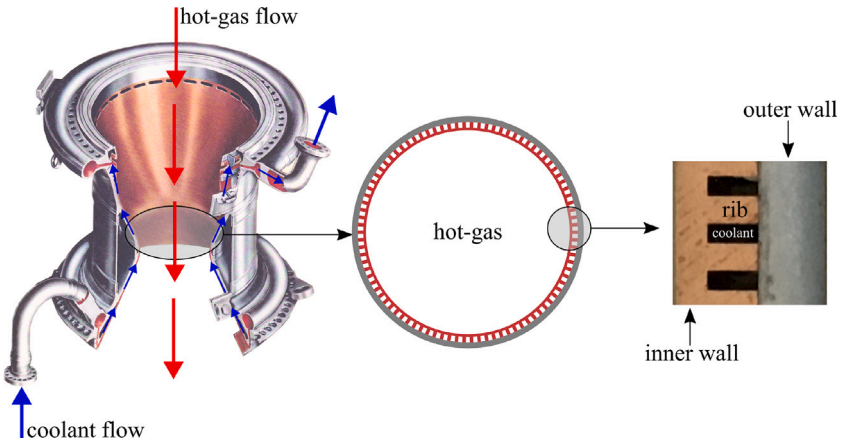


**Fig. 1.** Scheme of a conventionally-manufactured, regeneratively-cooled thrust chamber composed of two main materials, the inner one (in orange) with maximized thermal conductivity and the outer one (in gray) with maximized mechanical strength. Left: cut view of a thrust chamber (NASA courtesy) with indicated the hot-gas and the coolant flow. Center: cross-section with multiple cooling channels. Right: detail of a real cross-section, with indicated inner wall, ribs, and the outer wall (CIRA courtesy). (For interpretation of the references to color in this figure legend, the reader is referred to the web version of this article.)

## 3. Hot-gas side heat transfer

The importance of properly characterizing the heat transfer at the hot-gas side mainly relies on the need to estimate the maximum wall temperature and heat flux as well as the total wall heat transfer rate. While the first two parameters represent the limiting factors for the thrust chamber life, the latter is the essential input for the evaluation of important engine parameters like coolant pressure drop and temperature gain within the cooling system. In the early development phase of a new rocket engine, properly instrumented thrust chambers, often at a reduced scale in terms of geometry and combustion chamber pressure, are effective tools for evaluating the hot-gas side heat transfer and, possibly, comparing the effect of different injectors and thrust chamber designs on the heat transfer.

In the present review, experimental heat transfer studies are divided between those carried out using thrust chambers with “numerous” or “few” injection elements. Regardless of the exact quantification of the number of injection elements, the first case represents chambers that aim to be sufficiently representative of those of flight engines, albeit of relatively reduced size and pressure. The second case represents very down-sized chambers (thus, “few” injection elements) useful for characterizing in detail the heat transfer in the injection region.

### 3.1. Thrust chambers with numerous injection elements

The most adopted apparatus to measure the steady-state wall heat flux distribution in thrust chambers with relatively high chamber pressure is the calorimeter thrust chamber. This is a specially designed thrust chamber that consists of several axially segmented and independently water-cooled circuits. This enables the evaluation of the axial distribution of the heat transferred through the thrust chamber walls by metering the water mass-flow rate and measuring its temperature rise in each circuit. A schematic and a photo of the axial section of a calorimeter thrust chamber with multiple axial cooling circuits is shown in Fig. 2. A photo of the chamber assembled with the water inlet and outlet ducts feeding the axial cooling circuits is also shown in Fig. 2.

During the development of oxygen–methane booster engines made by NASA in late 1970s through the 1980s, several activities devoted to the hot-gas side heat transfer characterization were carried out using small-scale water-cooled calorimeter thrust chambers [5,19–21]. Because of the booster application, chamber pressure was often larger than 100 bar. In this framework, the heat flux to a chamber with a throat diameter of 8.4 cm was measured using a calorimeter chamber composed of 58 circumferential individual cooling circuits [5]. The injector was composed of 82 shear coaxial elements fed with a gaseous fuel rich mixture and liquid oxygen in order to be representative of a staged combustion feeding. The fuel was natural gas. Eight firing tests were conducted over a chamber pressure range from 83 to 145 bar and an oxidizer-to-fuel mass mixture ratio (henceforth called mixture ratio for simplicity) range from 2.5 to 3.6. The implementation of biasing the outer ring of injection elements (that is, the elements closest to the chamber wall) to a lower mixture ratio proved to be an effective method of reducing heating rates (Fig. 3).

The heat flux to the same calorimeter chamber was measured considering an injector composed of 60 coaxial elements with swirled liquid oxygen flow [19]. Methane was injected in gaseous form at ambient temperature. Nine firing tests were conducted over a chamber pressure range of 97 to 159 bar and mixture ratio varying between 2.5 and 3.4, showing an increased heat flux with increasing mixture ratio (Fig. 4).

A calorimeter thrust chamber having a throat diameter of 8.3 cm was used to measure the heat flux with and without a zirconium oxide (zirconia) coating applied on the hot-gas side of the chamber [20]. In fact, one way to reduce the heat flux is to use a thermal barrier, such as a ceramic coating, on the hot-gas side wall. The injector was composed of 82 shear coaxial elements fed with liquid oxygen and gaseous methane. The peak heat flux at the throat reduced by over 60% when using the zirconia coating (Fig. 5). However, this beneficial effect vanished soon because of the zirconia coating degradation as hot-fire time accumulated. In fact, the ceramic coating easily suffers spalling or flaws under high temperature gradient conditions due to the mismatch of the thermal expansion between the ceramic layer and the metal substrate.

Further heat transfer data were collected using a calorimeter chamber having a throat diameter of 9.1 cm and an injector composed of 58 shear coaxial elements injecting liquid oxygen and gaseous methane and a porous faceplate through which a small percentage of the gaseous methane mass flow rate was injected [21]. The nominal chamber pressure was 138 bar. The studied effect of the mixture ratio (Fig. 6) shows that the peak heat flux in the throat region increases as the stoichiometric condition (mixture ratio equal to 4) is approached because of the increased combustion temperature. Moreover, Fig. 6 also shows that an effective mean to reduce the heat transfer is the reduction of the mixture ratio of the injection elements facing the chamber wall (i.e., mixture ratio bias).

Within the same research activity [21], a film cooling was considered as a different mean to reduce the throat heat transfer. While the traditional film cooling is achieved by injecting fuel from suitable orifices present in the chamber liner close to the injector, i.e. far from the zone of maximum heat flux, a different solution was proposed. The film coolant was injected much closer to the throat, at the end

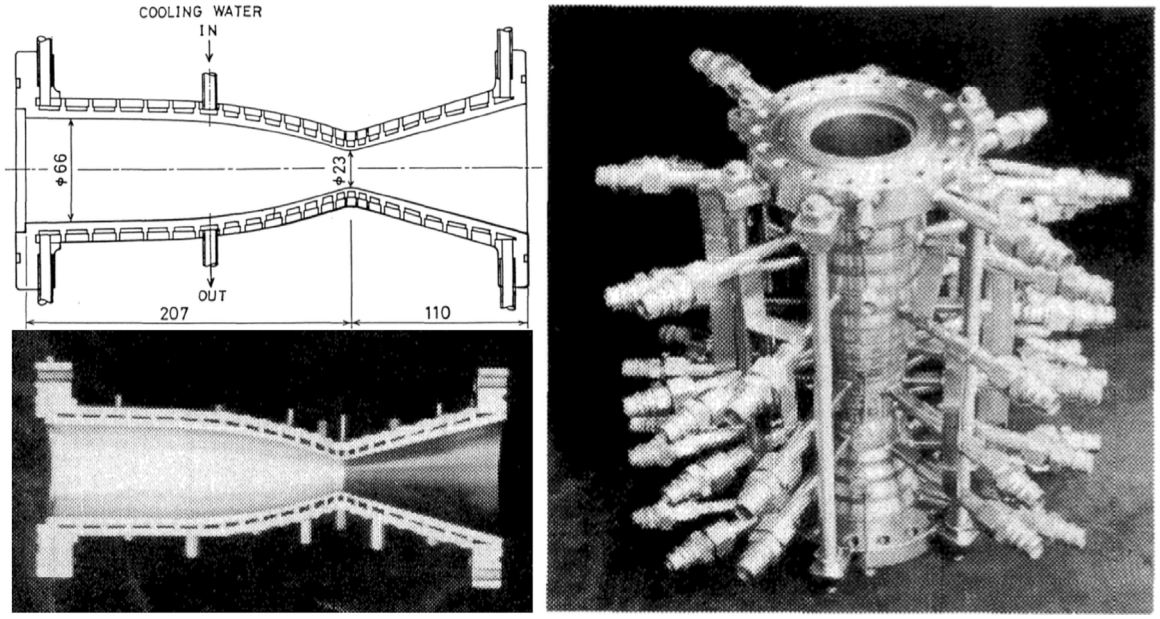


**Fig. 2.** A calorimeter thrust chamber with 23 independent circular cooling circuits. Upper-left: schematic of the axial section. Lower-left: photo of an axial cut. Right: photo of the chamber assembled with the water inlet and outlet ducts feeding the axial cooling circuits.
*Source:* (From [18]).

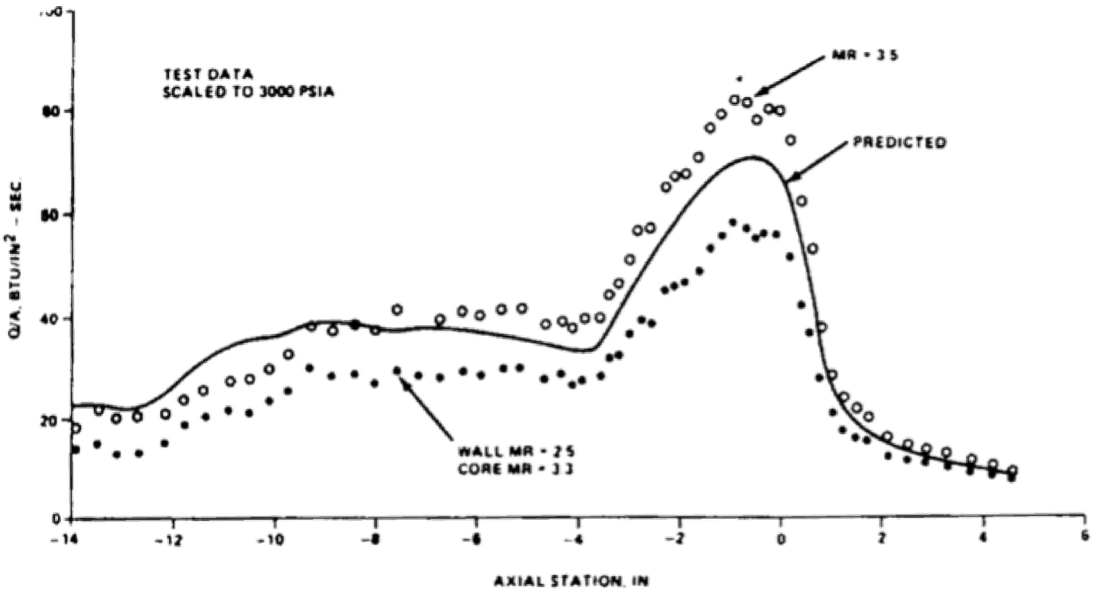


**Fig. 3.** Hot-gas side heat flux measurement using a calorimeter thrust chamber, with and without mixture ratio biasing. In case of homogeneous injection the mixture ratio is 3.5; in case of biased injection the mixture is 2.5 close to the chamber wall and 3.3 in the core region. The heat flux is scaled to 207 bar. On the x-axis: chamber axis in [in] ($x = 0$: throat section). On the y-axis: wall heat flux in [BTU/(in$^2$s)].
*Source:* (From [5]).

of the cylinder portion of the thrust chamber. Film coolant was liquid methane. Fig. 7 shows that using a small portion of the methane mass flow rate for this purpose can reduce dramatically the throat heat flux.

Relevant investigations of the hot-gas side heat transfer within thrust chambers having relatively high combustion pressure have been performed also in Japan. In [18,22] calorimeter chambers with a throat diameter of 23 mm and different cylinder section length were used to measure the axial heat flux distribution. The chamber pressure ranged from 31 to 96 bar and mixture ratio from 2.2 to 5.1. Six types of injectors having 18 coaxial type elements were tested. Four injectors had porous faceplate, which allowed fuel transpiration cooling, one had a solid copper faceplate with fuel film coolant holes, and one had both porous faceplate and film cooling holes. To be representative of a staged combustion feeding, liquid oxygen and a gaseous fuel rich mixture was injected. The fuel injection temperature ranged from ambient condition up to 1100 K. Significant carbon deposition was not observed although the surface of the hot-gas side wall was slightly blackened, and significant reduction of heat flux caused by carbon deposition on the chamber walls was also not detected. With similar calorimeter thrust chambers, injectors, and operative conditions, in [23] the characteristics of heat transfer to a nickel plated chamber walls was investigated. The study demonstrated that, even if such a coating might cause great thermal stress across the coated layer and result in separation of the two metals at their interface, the nickel plating is an effective means to reduce the heat transfer without evident detriment to the life of the chamber while experiencing multiple firing tests. In fact, the heat flux values

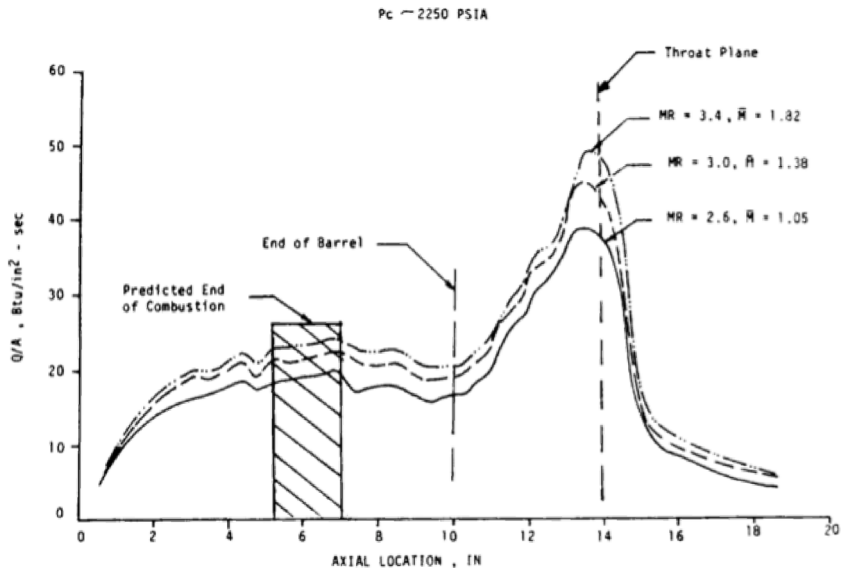


**Fig. 4.** Hot-gas side heat flux measurement using a calorimeter thrust chamber. Data are relevant to a chamber pressure of 155 bar and a mixture ratio ranging from 2.6 to 3.4. On the x-axis: chamber axis in [in] ($x = 0$: injector plate). On the y-axis: wall heat flux in [BTU/(in$^2$s)].
*Source:* (From [19]).

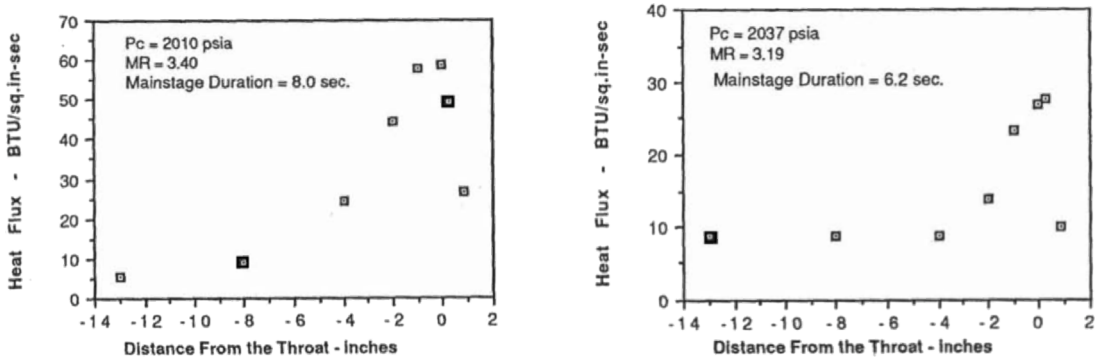


**Fig. 5.** Hot-gas side heat flux measurement using a calorimeter thrust chamber. Left: chamber pressure 139 bar, mixture ratio 3.4, without zirconia coating. Right: chamber pressure 140 bar, mixture ratio 3.19, with zirconia coating. On the x-axis: chamber axis in [in] ($x = 0$: throat section). On the y-axis: wall heat flux in [BTU/(in$^2$s)].
*Source:* (From [20]).

measured at the throat section of a nickel-plated chamber were 20% to 30% lower than values measured for a bare copper chamber. It was inferred that micro-cracks within the nickel layer relaxed thermal stress and prevented crack propagation. More recently, a calorimeter thrust chamber was used to characterize the heat transfer to the hot wall of an expander-cycle engine having a target combustion pressure of 47 bar and a mixture ratio 3.3 [24]. The injector had 36 coaxial type elements injecting liquid oxygen and gaseous methane. A porous plate manufactured by additive manufacturing was installed as a faceplate for the sake of fuel transpiration cooling and avoid damage of the injector. Five firing tests with accumulated burning time of 111 s were performed showing an increasing heat transfer with increasing combustion pressure.

The German Aerospace Center (DLR) studied the effect of film cooling using a calorimeter thrust chamber with a throat diameter of 28 mm and an initial cylinder section with a length of 100 mm [25]. The schematic of the DLR calorimeter thrust chamber and of the injector faceplate is shown in Fig. 8. The cylinder section was instrumented with thermocouples immersed within the wall in order to give a high-resolution temperature distribution in circumferential and axial directions. The injector was composed of 15 coaxial elements fed with liquid oxygen and gaseous methane. The elements were arranged in two rows: the inner one having 5 elements and the outer one having 10 elements. For film cooling investigations, the injector faceplate was surrounded by 10 evenly distributed cooling slots for tangential film coolant injection. The slots were put in correspondence of the injection elements of the outer row. Injected coolant was ambient temperature methane. Chamber pressure varied from 40 bar to 70 bar while the mixture ratio was kept constant to about 3.4. The measurements have shown that in the vicinity of the faceplate an effective reduction of the chamber wall temperature occurred while using a relatively small amount of coolant mass flow (about 1% of the total injected mass flow). The highest film cooling efficiency has been measured between the cooling slots because of the absence of an outer injection element in correspondence of that location. Moreover, no evident effect of the chamber pressure has been noted.

Since additive manufacturing is becoming a more and more promising realization process for rocket engines, in [26] a subscale thrust chamber realized in copper-based alloy by additive manufacturing has been tested by DLR in order to characterize the hot-gas side heat transfer. The thrust chamber, having a cylinder diameter of 80 mm, was fed with liquid oxygen and liquid methane with mixture ratio ranging from 3 to 3.8 and operated at a chamber pressure up to 80 bar. The thrust chamber was cooled by axial channels fed with water, whose temperature gain between inlet and outlet manifolds is a measure of the total heat pick-up from the hot-gas. Fig. 9-left shows the heat pick-up of the additive manufacturing thrust chamber compared to that of

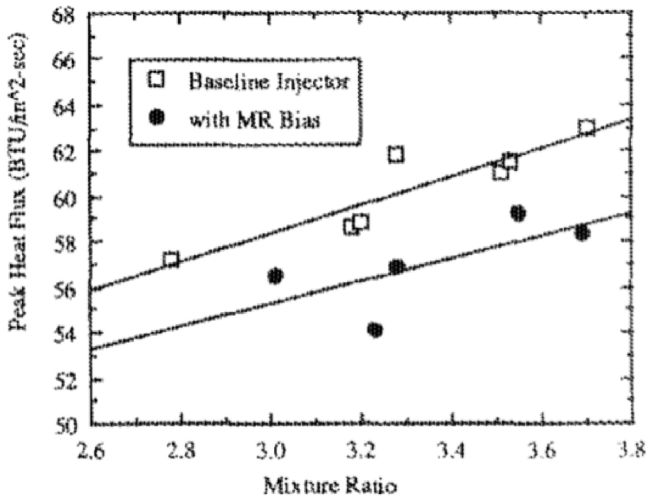


**Fig. 6.** Effect of the mixture ratio and the mixture ratio bias on the measured peak heat flux using a calorimeter thrust chamber with a chamber pressure of 138 bar. On the x-axis: mixture ratio. On the y-axis: peak wall heat flux in [BTU/(in$^2$s)].
*Source:* (From [21]).

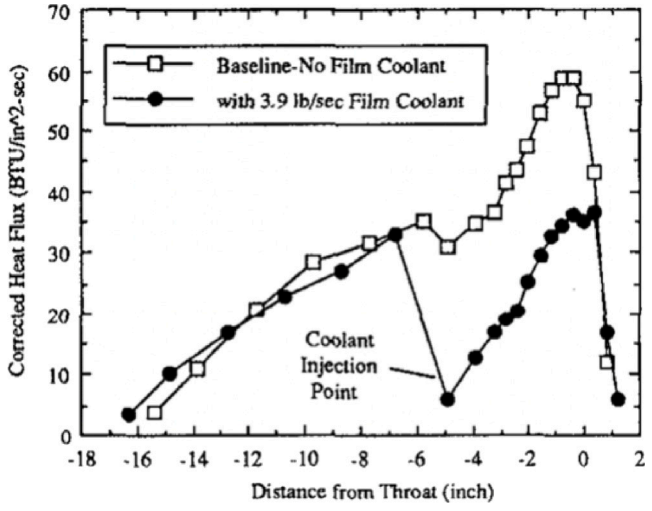


**Fig. 7.** Hot-gas side heat flux measurement using a calorimeter thrust chamber, with and without film cooling. Data are relevant to a chamber pressure of 138 bar. On the x-axis: chamber axis in [in] ($x$ = 0: throat section). On the y-axis: wall heat flux in [BTU/(in$^2$s)].
*Source:* (From [21])

an identical thrust chamber that was conventionally manufactured. The heat pick-up of the chamber made by additive manufacturing is at least 60% higher than in case of conventional chamber. This is a consequence of the poor surface finish quality that is inherent in additive manufacturing. In fact, the geometrical surface roughness at the hot-gas side was about 1 μm for the conventional manufacturing and, on average, about 10 μm for the additive manufacturing. However, Fig. 9-right shows that, as the test campaign progressed with hot-fire tests, the heat pick-up of the additive manufacturing chamber decreased by more than 10% as a consequence of the decrease in roughness down to, on average, 6 μm at the end of the test campaign. This smoothing of the surface was presumably induced by the flow of hot-gas.

The experimental data of [18–21] and relevant to the peak heat transfer in the throat region of oxygen–methane thrust chambers have been displayed in Fig. 10 in terms of non-dimensional numbers evaluated using free-stream hot-gas properties. The detailed methodology for data selection and elaboration is provided in [27]. Here it is worth recalling that cases with film cooling or intended non-uniform injection (e.g., mixture ratio bias) are not considered. The heat transfer correlation that best fits the 36 collected test data is:

$$Nu = 0.0296 Re^{0.8} Pr^{0.4} \tag{1}$$

where $Nu$ is the Nusselt number, $Re$ is the Reynolds number, and $Pr$ is the Prandtl number. Fig. 10 also shows that, to include 95.45% of the data, the coefficient 0.0296 must be increased to 0.0372, that is, by about 25%. The two correlations are labeled as "fitting" and "+2$\sigma$" in that Figure. The study [27] demonstrates that there are no substantial differences in the description of heat transfer compared to other propellant combinations like oxygen–hydrogen and oxygen–kerosene, as the correlation formulas for such propellant combinations are very similar to Eq. (1). Finally, note that, although the above correlation is fit to the data pertinent to the throat region, it can be used as a first attempt for the other thrust chamber sections as well.

### 3.2. Thrust chambers with few injection elements

The effect of the injection elements configuration on the heat transfer in the initial part of the thrust chamber, that is, where the flame develops, is often studied in small chambers that are fed with few injection elements. Such apparatuses do not necessitate complex and costly equipment and are suited to accurate and massive instrumentation and easy variation of configuration and operative conditions. To further simplify the configuration and operability of the apparatuses, a heat-sink sink chamber is often considered (i.e., no active cooling). In such type of chambers, multiple thermocouples are immersed within the thickness of the chamber such that the time evolution of the wall temperature permits to evaluate the heat flux and the heat transfer coefficient, both in the axial and circular directions. Although the limited heat capacity of the chamber limits the chamber pressure and the firing duration to few seconds, the wall temperature transient data permits to properly characterize the behavior of the steady state heat transfer.

In the last decade, the Technical University of Munich (TUM), has carried out numerous experimental studies on the heat transfer in the region immediately downstream of the propellant injection using mainly, but not limited to, heat sink chambers [28]. Chambers were used with different number of injection elements (from single element up to 7), arrangement of injection elements, and geometry of the cross-section (circular, square, or rectangular). The schematics of the single-element heat-sink chamber with square section and of the 7-elements calorimeter chamber with circular section are shown in Fig. 11. The adopted chambers have the following characteristic features in common: ambient temperature gaseous propellants, identical shear coaxial injection elements, identical injection elements to wall distance of 3 mm, and identical nozzle contraction ratios which guarantee a Mach number of 0.25 in the cylinder section of the chamber. The combustion chamber pressure was varied from 5 bar to 50 bar. Fig. 12 shows the wall heat flux developing with the flame formation within the single-element, square-section chamber [29]. Because of the fuel-to-oxidizer velocity and momentum ratio decrease with increasing mixture ratio when injecting gaseous propellants, the propellant mixing and the consequent heat transfer is expected to increase with decreasing mixture ratio. This phenomenon is only partially noticeable in Fig. 12-left, perhaps due to the relatively small variation of the experimented mixture ratio. On the other hand, the effect of the pressure is far more evident (Fig. 12-right). Here, the main reason for heat flux increase is the increasing mass flux with increasing pressure. In [29] it is affirmed that the heat flux is about proportional to the pressure at the power of 0.8, as foreseen when the heat is transmitted by turbulent convection. Similar results about the effect of the mixture ratio and the chamber pressure have been experienced with the multi-elements calorimeter chamber [30] (Fig. 13). In such a case, is it worth noting that the nozzle heat flux (i.e., measured with the calorimeter located after

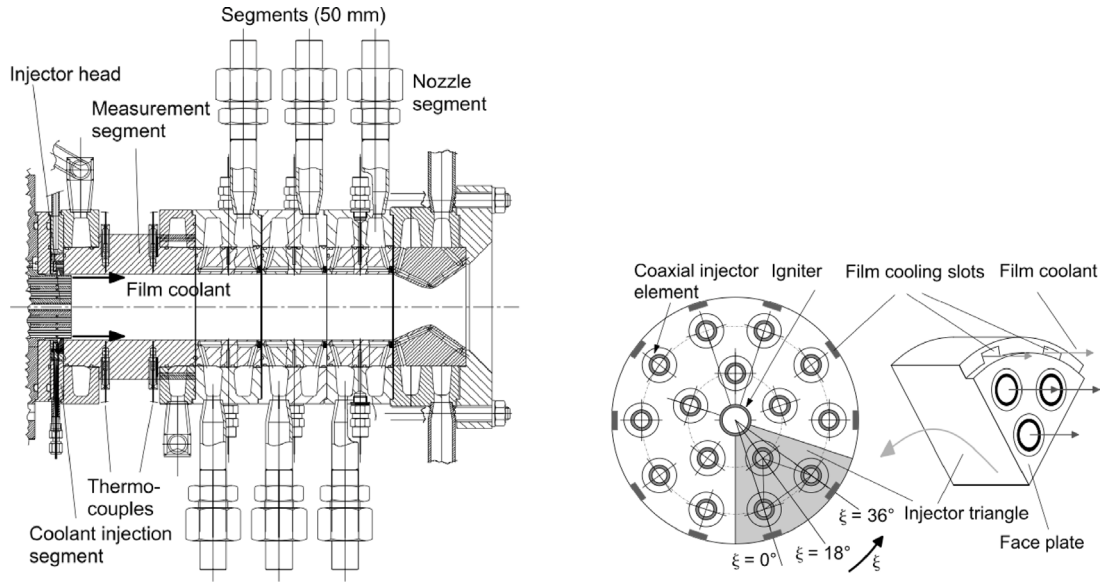


**Fig. 8.** The DLR calorimeter thrust chamber with film cooling. Left: the schematic of the chamber axial section showing the water cooled segments and the initial cylinder section with immersed thermocouples. Right: the schematic view of the injector faceplate showing the coaxial injection elements and the peripheral film cooling slots.
*Source:* (From [25]).

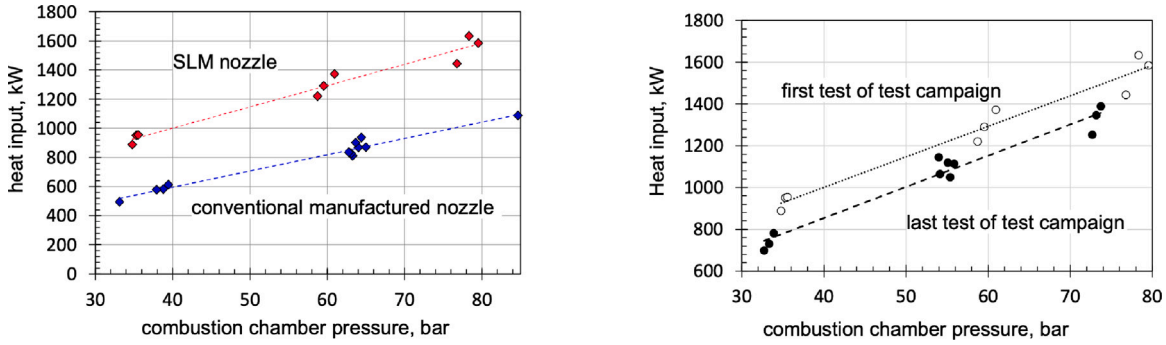


**Fig. 9.** Left: comparison of heat pick-up of a conventional and an additive manufacturing thrust chamber at different combustion pressures. Right: evolution of the heat pick-up of the additive manufacturing thrust chamber at different combustion pressures during the progress of the test campaign. On the x-axis: chamber pressure in [bar]. On the y-axis: heat peak-up in [kW].
*Source:* (From [26]).

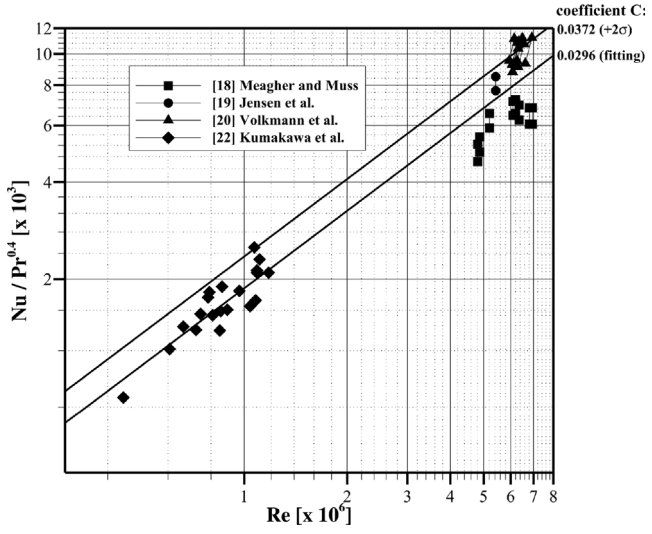


**Fig. 10.** Throat heat transfer behavior of the data relevant to the oxygen–methane propellants, grouped by literature source, in terms of non-dimensional numbers evaluated using free-stream hot-gas properties.

about 340 mm, Fig. 13) increases with increasing mixture ratio. Here the flame is completely developed and the phenomenon that drives the heat transfer is the adiabatic flame temperature, which increases approaching the stoichiometric condition (mixture ratio equal to 4).

In addition to the studies on the effect of the mixture ratio and chamber pressure, the single-element circular cross-section chamber has been used by TUM to study the effect of the oxygen post recess, that is, the space in which the propellants of an element mix before entering the main chamber. A schematic of the adopted injection element with oxygen post recess of length $R$ is shown in Fig. 14. In [31] it has been observed that the oxygen post recess enhances the mixing between the propellants, and thus the heat flux, when its length is longer than about 1 post exit diameter (Fig. 15). On the other hand, for recess lengths smaller than the oxygen post diameter there is a tendency to develop flow instabilities due to lifted flames. Such flow instability results in a characteristic pattern with very high temperatures where the flame is bouncing back and forth.

The Pennsylvania State University tested three type of injection elements in a 2.5 cm diameter circular cross-section chamber operating with liquid oxygen and gaseous methane [32]. The tested injection elements were two versions of a shear coaxial element and a swirl coaxial element. The two tested shear coaxial elements differed in the fuel-to-oxidizer momentum flux ratios. Tested chamber pressure

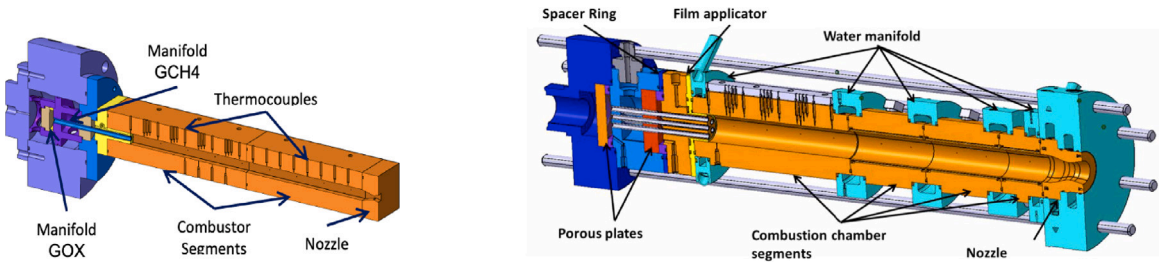


**Fig. 11.** Schematics of the TUM chambers. Left: the single-element heat-sink chamber with square cross-section. Right: the 7-elements calorimeter chamber with circular cross-section. *Source:* (From [28]).

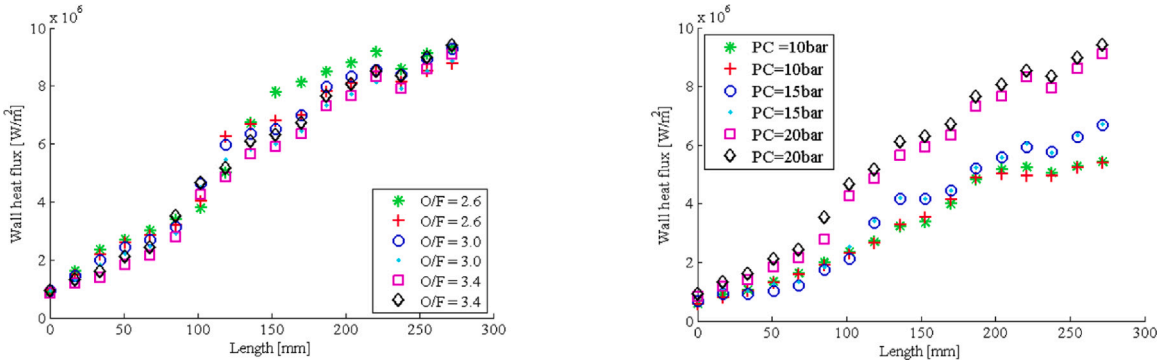


**Fig. 12.** Wall heat flux distribution along the axis of a single-element, square-section chamber at constant chamber pressure equal to 20 bar but variable mixture ratio (left) and at constant mixture ratio equal to 3.4 but variable chamber pressure (right). On the x-axis: chamber axis in [mm] ($x = 0$: injector plate). On the y-axis: wall heat flux in [MW/m$^2$]. *Source:* (From [29]).

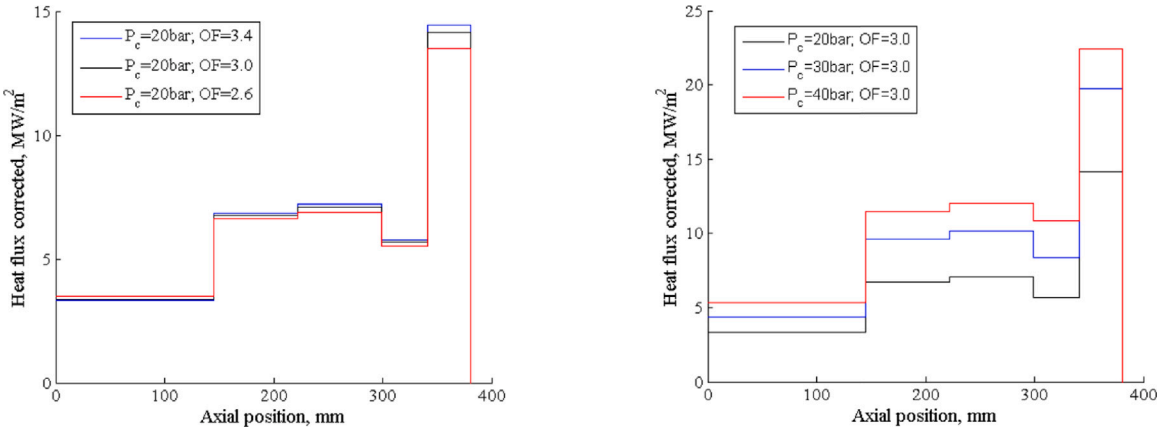


**Fig. 13.** Average wall heat flux in the five axial segments of a 7-elements, circular-section calorimeter thrust chamber at constant chamber pressure equal to 20 bar but variable mixture ratio (left) and at constant mixture ratio equal to 3.0 but variable chamber pressure (right). On the x-axis: chamber axis in [mm] ($x = 0$: injector plate). On the y-axis: wall heat flux in [MW/m$^2$]. Note: the calorimeters before about 340 mm are cylindrical, while the last one contains the nozzle. (For interpretation of the references to color in this figure legend, the reader is referred to the web version of this article.)
*Source:* (From [30]).

ranged from 21 to 83 bar and the mixture ratio ranged from 2.5 to 3.25. Results relevant to 69 bar and mixture ratio 3.0 are reproduced in Fig. 16. The measurements indicated a higher heat flux levels for the swirl coaxial element than the two versions of the shear coaxial element at near injector face locations. This is attributed to enhanced liquid oxygen atomization, mixing, and combustion provided by the conical swirling spray for the swirl coaxial element. The shear coaxial element with the higher fuel-to-oxidizer momentum flux ratio showed higher heat flux levels in the near injector face region. Moreover, one of the two shear coaxial elements was designed such that the oxygen post could be configured flush or recessed with respect to the injector face. The configuration with the oxygen post recessed showed higher heat flux levels in the near injector face region than its oxygen post flush counterpart, indicating that the mixing cup provided by recessing the oxygen post has a positive effect on the mixing and combustion characteristics of the injector.

A test series aimed at investigating the heat fluxes in the cylindrical portion of a subscale thrust chamber operated with oxygen and methane was achieved at the Mascotte test facility, Onera, France [33]. The chamber, which has a cylindrical portion with a diameter of 5.6 cm and a length of about 40 cm, was fed with five shear coaxial injection elements, a central one and four arranged circularly around the axis of the chamber. A total of nearly one hundred and fifty operating points were reached, enabling to cover a wide operating domain, ranging chamber pressure from 20 bar to 70 bar and mixture ratio up to 3.5. Methane was always injected gaseous at ambient temperature, while oxygen was either gaseous at room temperature or liquid at approximately 100 K. By using an interchangeable faceplate, the influences

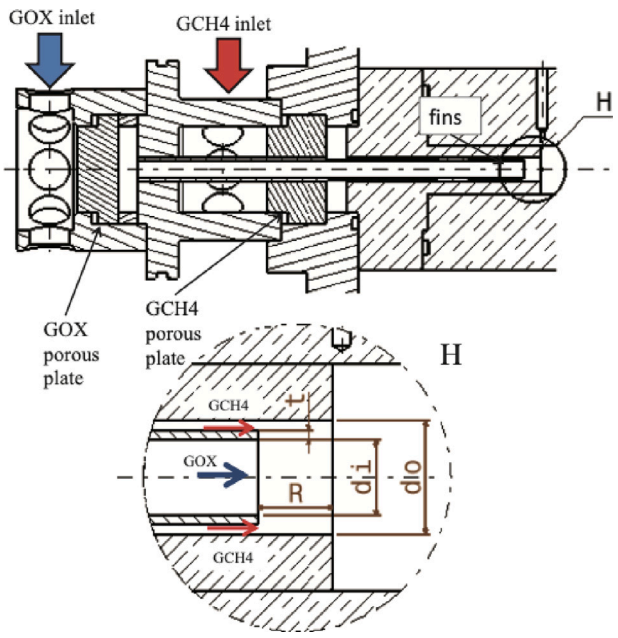


**Fig. 14.** Schematic of the detail of the TUM injection element with oxygen post recess of length $R$.
*Source:* (From [31]).

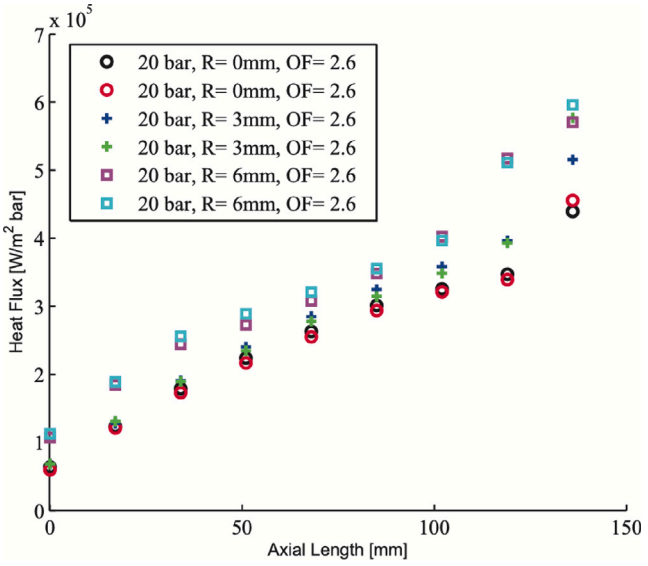


**Fig. 15.** Wall heat flux distribution along the axis of the single-element, circular-section chamber at constant chamber pressure and mixture ratio (20 bar and 2.6, respectively) and different oxygen post recess length: 0 (i.e., flush post), 3 mm, and 6 mm (the oxygen post exit diameter is 4 mm). On the x-axis: chamber axis in [mm] ($x = 0$: injector plate). On the y-axis: wall heat flux in [MW/m$^2$].
*Source:* (From [31]).

of geometrical parameters like the injection elements diameter and the distance between the injection elements and the wall were investigated. As shown in Fig. 17-left, in case of gas/gas injection the heat flux increased with both chamber pressure and mixture ratio. Such expected result is similar, both qualitatively and quantitatively, than the case of gas/gas injection of oxygen/hydrogen. On the other hand, in case of liquid/gas injection the behavior seems to change drastically (Fig. 17-right). The heat flux is relatively lower than the case of liquid/gas injection of oxygen/hydrogen. Such behavior may be attributed to incomplete oxygen/methane combustion.

## 4. Coolant heat transfer and wall compatibility

When dealing with regenerative thrust chambers, the turbulent flow within the cooling channels ensures that such component operates within an acceptable temperature range. Obviously, the characterization of the coolant heat transfer, as well as the coolant compatibility with the channels material, is essential to verify the feasibility of a thrust chamber design. Because of the inherently complexity and high cost in directly measuring the coolant heat transfer in a thrust chamber, heated tube experiments are very common. Such type of experiment consists of flowing a known coolant flow rate into a heated channel and measuring the temperature gain between the channel inlet and outlet and the wall temperature at various stations. This makes it possible to calculate, especially in the simplified case of a straight channel with circular cross-section (which is typically called a “tube”), the convective heat transfer coefficient of the coolant along the channel length. Multiple measurements of this coefficient are then used to find non-dimensional heat transfer correlations using fluid properties evaluated at both the bulk and the wall temperature. To better represent the operating conditions of a thrust chamber, channels with a rectangular section and with asymmetrical heating are sometimes considered even if in this case the definition of the heat transfer coefficient is less obvious due to the three-dimensional nature of the temperature field (both in the material and in the coolant flow). The reported experimental studies are divided with respect to the value of the critical pressure. Since the fuel is used as a coolant, it is worth recalling that the critical pressure of pure methane is about 46 bar. In the case of supercritical pressure, typical of chambers fed with pumps, the fluid is single-phase while in the subcritical case the fluid is two-phase (liquid and vapor). In this second case, in addition to the heat transfer coefficient, it is important to identify the critical heat flux. This value identifies a thermal limit beyond which there is a sudden phase change due to boiling, often leading to a deterioration of the heat transfer with a consequent dangerous increase in the wall temperature. The identification of this parameter is obviously important for the design of combustion chambers operating at relatively low pressure. In addition to the studies on the heat transfer, those relating to the compatibility between the coolant and the material of the channels are also reported.

### 4.1. Heat transfer characteristics at supercritical pressure

Using an electrically heated circular tube, an heat transfer correlation for natural gas (96.5 mol% methane) was found by NASA [34]. The tube had an inner diameter of about 1.96 mm and a length of about 25 cm. Two different materials were used for the tube inner surface: copper or nickel-plated copper. Most of the tests were carried out with an inlet velocity of about 30 m/s and an inlet pressure of about 130 bar. Tests were performed with both ambient and cryogenic inlet temperature natural gas. The measured maximum wall temperature was about 860 K. Fig. 18 shows that the 130 experimental data, taken during the steady-state condition of the 12 performed tests, can be described within 30% of uncertainty by the formula:

$$Nu_b = 0.0028\, Re_b Pr_b^{0.4} \left(\frac{\rho_b}{\rho_w}\right)^{1.5} \left(\frac{\mu_b}{\mu_w}\right)^{-6.5} \left(\frac{k_b}{k_w}\right)^{6.4} \left(\frac{\bar{c}_p}{c_{p,b}}\right)^{2.4} \left(1 + \frac{2}{x/D}\right) \tag{2}$$

where the subscripts $b$ and $w$ mean that the coolant properties are evaluated at the bulk temperature $T_b$ and at the wall temperature $T_w$, respectively. Moreover, $\rho$, $\mu$, and $k$ are the coolant density, dynamic viscosity, and thermal conductivity, respectively, and $\bar{c}_p$ is the average value of the fluid specific heat at constant pressure computed from the wall temperature and the bulk temperature. Finally, $x$ is the distance from the heated tube inlet, and $D$ is the tube diameter.

A further heat transfer correlation for pure methane and natural gas (92.5 mol% methane) was found by NASA [35,36]. The electrically

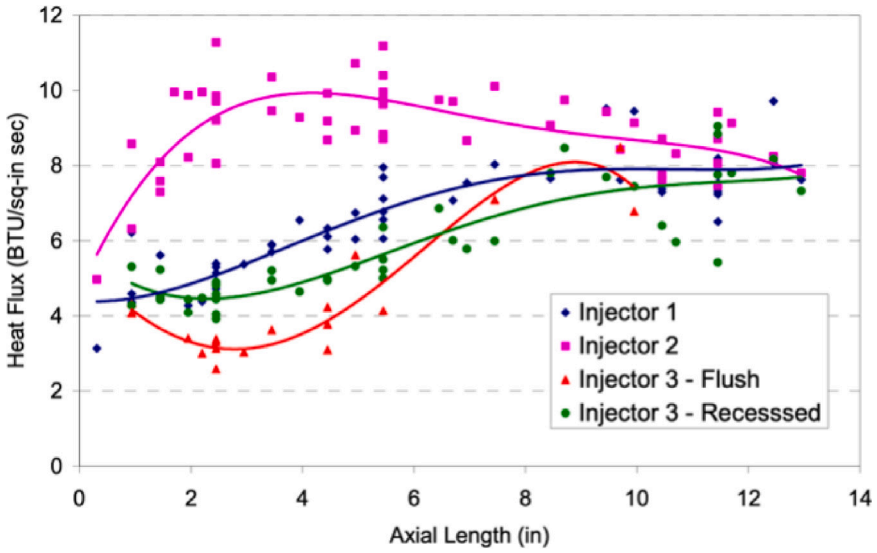


**Fig. 16.** Wall heat flux profiles for three injection elements at chamber pressure of 69 bar and mixture ratio of 3.0. Injector 1: shear coaxial element with higher fuel-to-oxidizer momentum flux ratio; injector 2: swirl coaxial element; injector 3: shear coaxial element with lower fuel-to-oxidizer momentum flux ratio and with flush or recessed oxygen post. On the x-axis: chamber axis in [in] ($x = 0$: injector plate). On the y-axis: wall heat flux in [BTU/(in$^2$s)]. (For interpretation of the references to color in this figure legend, the reader is referred to the web version of this article.)
*Source:* (From [32]).

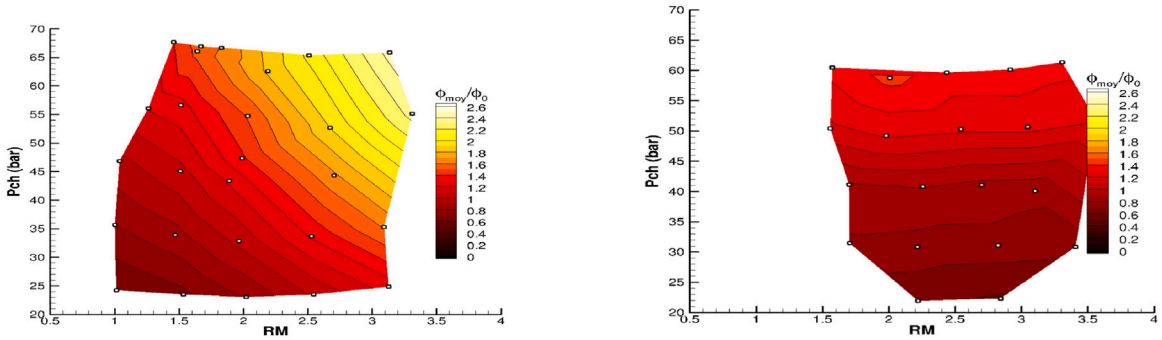


**Fig. 17.** Non-dimensional wall heat flux maps for gas/gas injection (left) and liquid/gas injection (right). The wall heat flux is averaged along the cylinder portion of the chamber. On the x-axis: mixture ratio. On the y-axis: chamber pressure in [bar].
*Source:* (From [33]).

heated tubes, made of copper, had an inner diameter of about 1.85 mm and a length of up to 18 cm. Both smooth and rough tubes were used. In the latter case, the geometric surface roughness was 0.4 μm. The coolant inlet temperature ranged from 146 K to 275 K, the inlet pressure from 270 bar to 342 bar, and the inlet velocity from 55 m/s to 238 m/s. The heat flux entering the coolant was up to 139 MW/m$^2$. A total number of 450 steady-state data points have been originated by 37 tests. The proposed heat transfer correlation for methane and natural gas in smooth tubes is:

$$Nu_b = 0.022 Re_b^{0.8} Pr_b^{0.4} \left(\frac{T_b}{T_w}\right)^{0.45} \tag{3}$$

Incorporating the wall roughness, the proposed heat transfer correlation is:

$$Nu_b = 0.4 \frac{(f/8)\, Re_b Pr_b}{1 + \sqrt{f/8}\left(5.19\varepsilon^{0.2} Pr_b^{0.44} - 8.5\right)} \tag{4}$$

where $f$ is the friction factor and $\varepsilon$ is the equivalent sand grain roughness. The whole data set is shown in Fig. 19, where it is evident the heat transfer enhancement induced by wall roughness.

The above studies [34–36] were performed using circular cross-section cooling channels that are homogeneously heated by ohmic heating. In [37] more representative conditions were reproduced by US researchers. The throat section of a two-dimensional combustor was cooled by rectangular cooling channels, whose methane flow was orthogonal to that of the hot-gas, as shown in the schematic reported in Fig. 20. The geometry and the material of the channels was similar to that used on the Space Shuttle Main Engine thrust chamber. Four thermocouples were brazed into the channel ribs to provide coolant side wall temperature data. The hot-gas side conditions were representative of a rocket engine operating at relatively high chamber pressure (140 bar and more). Coolant velocity, wall temperature, and heat flux were varied parametrically during the test program. Fig. 21 shows that the best heat transfer correlation for methane in such rectangular cooling channels is:

$$Nu_b = 0.031 Re_b^{0.8} Pr_b^{0.4} \left(\frac{T_b}{T_w}\right)^{0.47} \tag{5}$$

Fig. 21 also evidences that a correlation very similar to Eq. (3) underestimates the experimental data. However, the difference between the two correlations may be partly due to the difficulty of defining a unique value of the wall temperature in the case of a rectangular channel. Indeed, in [37] it is clarified that, since the temperature of the wall varies around the channel periphery, an average heat transfer coefficient was used in the determination of the Nusselt number.

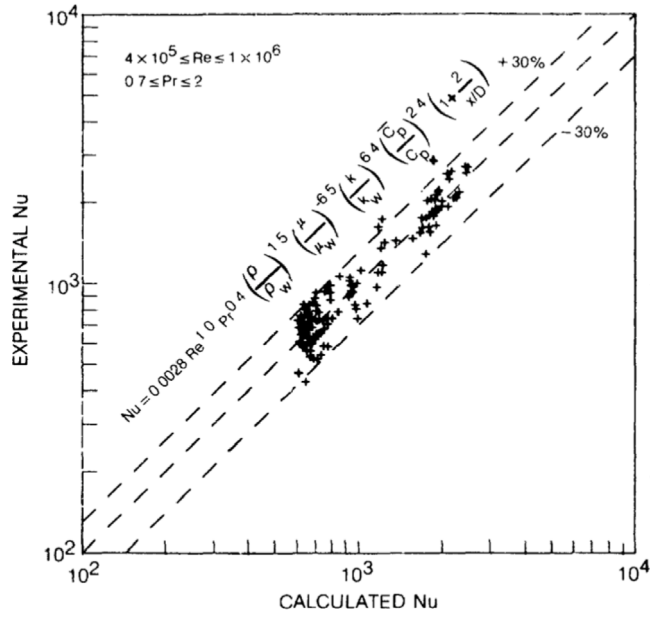


**Fig. 18.** Natural gas heat transfer data for circular tubes. On the x-axis: the computed Nusselt number using Eq. (2). On the y-axis: the experimental Nusselt number. *Source:* (From [34]).

In [38], more than 10000 data obtained by Chinese researchers using a heated tube apparatus suggest that for a Reynolds number range from $3.5 \cdot 10^4$ to $3 \cdot 10^6$ the methane heat transfer is fairly correlated with the so called Dittus-Boelter equation:

$$Nu_b = 0.023\, Re_b^{0.8}\, Pr_b^{0.4} \tag{6}$$

Even if the above correlation does not contain any direct wall temperature effect, a decrease of heat transfer at high wall temperatures was experimentally measured. The tests were conducted using stainless steel and copper circular tubes having an inner diameter of 3 mm. Methane operates at pressures from 5 to 260 bar, at temperatures from 128 to 196 K, and flow velocities from 2 to 106 m/s. Maximum reached wall heat flux was 66 MW/m$^2$. In [39] the heat transfer of supercritical cryogenic methane in a stainless steel electrically heated circular tube having an inner diameter of 2.6 mm was experimentally investigated by a further team of Chinese researchers. Experimental conditions included pressures from 50 to 150 bar, mass fluxes from 6000 to 15000 kg/(m$^2$ s), and heat fluxes up to 16 MW/m$^2$. Fig. 22 shows that, using Eq. (6), only 73% of the collected data can be described within ±25% of uncertainty. Moreover, such correlation tends to overestimate the heat transfer.

In [40], a heated tube apparatus was used by Japanese researchers to evaluate the heat transfer of liquid and gaseous methane. Fig. 23 shows that the Dittus-Boelter equation (6) correlates fairly the experimental heat transfer of gaseous methane. On the other hand, the experimental liquid methane data are far less correlated by the Dittus-Boelter equation (6), especially for Nusselt number higher than about 1500.

To study the heat transfer phenomena in cooling channels under real operative conditions, DLR performed tests using a cylindrical combustion chamber fed with 42 coaxial injection elements [41]. The chamber was divided into four sections around the circumference, each containing rectangular cooling channels with different aspect ratios (height-to-width ratio) equal to 1.7, 3.5, 9.2, and 30, respectively. The chamber was made of a copper-based alloy with channels closed by electrodeposit copper and then nickel. The surface of the cooling channels had an equivalent sand grain roughness of 0.2 μm. Liquefied natural gas, having a methane content larger than 98%, entered the cooling channels at a temperature as low as 130 K and at a pressure between 58 and 120 bar. The combustion chamber hot-gas flow exerted a wall heat flux up to 18 MW/m$^2$. One of the main goals of such study was the identification of the heat transfer deterioration onset. In fact, in analogy with the film boiling phenomena occurring at subcritical pressure, a supercritical fluid operating relatively close to the critical pressure may exhibit heat transfer deterioration. Such deterioration was identified in [41] monitoring the wall temperature measured by wall-immersed thermocouples. Test results indicated that cooling channels with a lower aspect ratio were more prone to this effect, as it occurred for smaller values of coolant heat-to-mass flux ratio, as shown in Fig. 24. Moreover, as expected, as the pressure was increased, deterioration tended to reduce as a result of the departure from the pseudo-boiling phenomena occurring close to the critical pressure. The acquired experimental data were also used to correlate the methane heat transfer in rectangular cooling channels [42]. The resulting correlation, depending on the channel aspect ratio $AR$, is:

$$Nu_b = \left(0.0286 \cdot e^{-0.0238AR} - 0.0046\right) Re_b^{0.8}\, Pr_b^{0.4} \left(\frac{T_b}{T_w}\right) \tag{7}$$

where the heat transfer coefficient was evaluated averaging the hot-gas side heat flux over the channel perimeter and $T_w$ is the hot-gas side wall temperature. Fig. 25 shows that uncertainty of the above correlation is below ±25% for 84% of the data. The accuracy strongly depends on the distance to the critical point. In fact, the larger deviations from the proposed correlation are found for the test cases closer to the critical pressure [42].

In [43] CIRA, Italy, investigated methane heat transfer by means of a test article composed of a copper-based alloy block warmed up by cartridge heaters and of a single channel with rectangular cross-section. The channel aspect ratio was 3. Tests were conducted with methane mass flux ranging from 3500 to 8500 kg/(m$^2$ s), exit pressure from 60 to 150 bar, and inlet temperature of about 130 − 140 K. The maximum provided heat flux at channel bottom was 20 MW/m$^2$. The resulting Reynolds number ranged from $9 \cdot 10^4$ to $8 \cdot 10^5$, the Prandtl number from 1.4 to 4, and the wall-to-bulk temperature ratio from 1.5 to 2.5, where the wall temperature is the estimation of the hot-gas side wall temperature of an equivalent thrust chamber with an inner layer thickness of 1 mm. The channel equivalent sand-grain surface roughness was estimated to be about 10 μm. Such non-negligible value of the roughness led to a greater heat transfer compared to the case with smooth surfaces. No tests have exhibited heat transfer deterioration, neither in the cases with lowest pressure (i.e., about 60 bar). The experimental heat transfer data can be correlated by the formula:

$$Nu_b = 0.032\, Re_b^{0.8}\, Pr_b^{-0.144} \left(\frac{T_b}{T_w}\right)^{0.539} \tag{8}$$

where, as already done in [42] for rectangular cooling channels, the heat transfer coefficient is evaluated averaging the hot-gas side heat flux over the channel perimeter. Fig. 26 shows that most of the experimental data (about 78%) are described by Eq. (8) with an uncertainty below 10%. Considering also the estimated experimental error, equation (8) fairly describes the measured heat transfer within ±25%. The maximum deviation is found for the cases with lowest pressure (about 60 bar).

### 4.2. Heat transfer characteristics at subcritical pressure

Methane critical heat flux was studied by NASA [44] conducting electrically heated tube tests characterized by flow velocities from 2.5 to 48 m/s, inlet pressures from 16 to 55 bar, and inlet temperature from 104 to 142 K. Three different Inconel 600 circular tubes, with nominal inner diameters of 0.65, 1.37, 1.91 mm, were used. The critical heat flux values were determined where the fluid transitions from nucleate boiling to film boiling. A typical behavior of the critical heat flux increasing with the product of the flow velocity and subcooling is

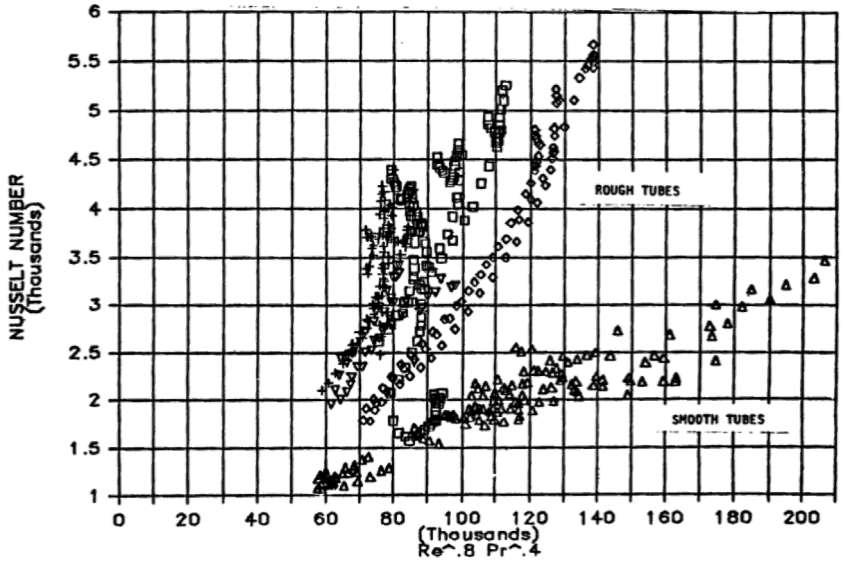


**Fig. 19.** Methane and natural gas heat transfer data for smooth and rough circular tubes. On the x-axis: the number $Re_b^{0.8} Pr_b^{0.4}$. On the y-axis: the experimental Nusselt number. *Source:* (From [36]).

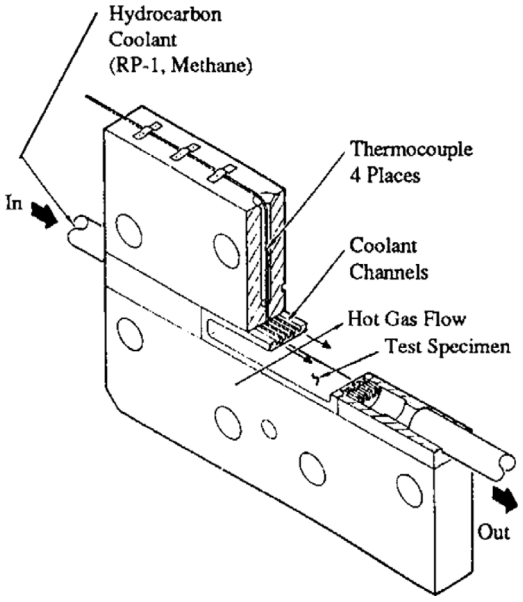


**Fig. 20.** Schematic of the throat section of the two-dimensional combustor investigated in [37], showing the rectangular cooling channels orthogonal to the hot-gas flow and the immersed thermocouples.
*Source:* (From [37]).

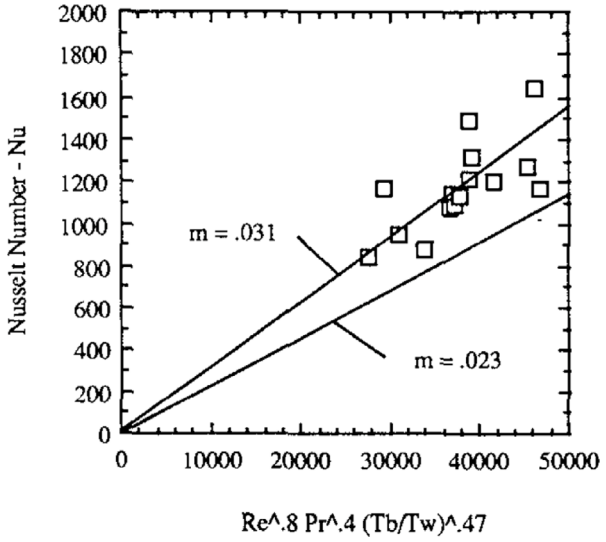


**Fig. 21.** Methane heat transfer data for rectangular cooling channels. On the x-axis: the number $Re_b^{0.8} Pr_b^{0.4} \left(\frac{T_b}{T_w}\right)^{0.47}$. On the y-axis: the experimental Nusselt number.
*Source:* (From [37]).

shown in Fig. 27. In this context, subcooling is defined as the difference between the saturation temperature at the operative pressure and the fluid bulk temperature, $T_{sat} - T_b$.

To investigate operative conditions closer to rocket engine cooling, square and rectangular single cooling channels fed with liquid methane and asymmetrically heated by means of heating cartridges have been tested by the University of Texas, USA [45]. The cooling channels, having a heated length of 5.1 cm, were made of a typical copper-based alloy used for rocket engine thrust chambers. Different channels were tested: a rectangular channel with a cross-section of 1.8 mm × 4.1 mm (base × height) and four square channels with a cross-section of 3.2 mm × 3.2 mm but different surface roughness. Tests with subcooled methane were conducted over a range of pressures from 10 to 21 bar and fluid velocities ranging from 7.1 to 14.3 m/s. Fig. 28 shows that film-boiling onset at critical heat flux was correlated to the Boiling number value of approximatively 0.1, where the Boiling number is defined as the ratio of the average entering heat flux to the product of the coolant mass flux and heat of vaporization. This result, shown in Fig. 28 for the rectangular channel, remains valid also for square channels with different surface finishes even if the results are more scattered in this case.

The test campaign presented in [45] provided also methane heat transfer data, which are presented in Fig. 29 in terms of the experimental Nusselt number as a function of $Re_b^{0.8} Pr_b^{0.4} \left(\frac{T_b}{T_w}\right)^{0.45}$. Although this parameter seems to correlate the Nusselt number fairly for the smooth cases, the heat transfer did not increase with increasing surface roughness, which disagrees with the expected trend. An increased heat transfer is evident only in the liquid non-boiling regime for a surface roughness level of 6.4 μm.

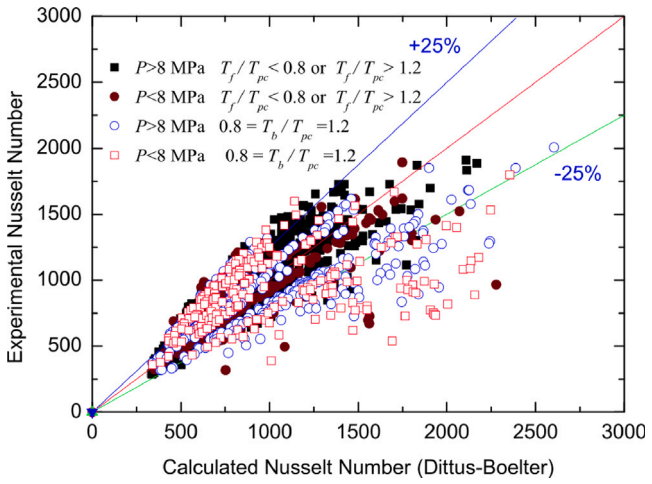


**Fig. 22.** Methane heat transfer data for circular tubes. On the x-axis: the computed Nusselt number using Eq. (6). On the y-axis: the experimental Nusselt number.
*Source:* (From [39]).

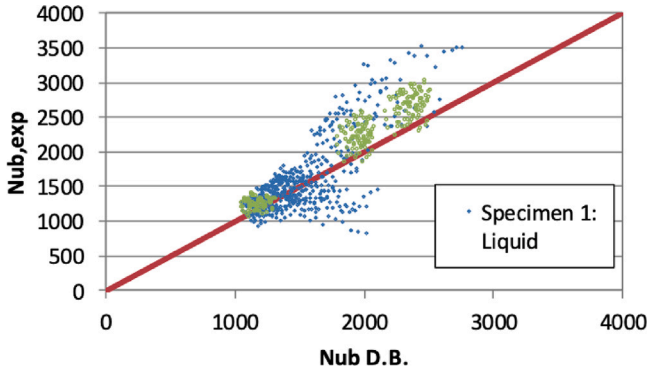


**Fig. 23.** Methane heat transfer data for circular tubes. On the x-axis: the computed Nusselt number using Eq. (6). On the y-axis: the experimental Nusselt number. Green points: gaseous methane data. Blue point: liquid methane data. (For interpretation of the references to color in this figure legend, the reader is referred to the web version of this article.)
*Source:* (From [40]).

### 4.3. Coolant wall compatibility

Within the research activities performed by NASA in [34–36] and described in Section 4.1 for the results relevant to the heat transfer behavior, the thermal stability of natural gas was also investigated. Corrosion of the copper tube surface was detected, possibly due to reactions with the trace sulfur impurities present in the coolant. In particular, in [34] the rates of carbon deposition (i.e., coke deposition) in copper tubes did not exceed 80 μg/(cm$^2$hr) at wall temperatures between 500 and 650 K. This deposition rate was four times lower than kerosene (more than 300 μg/(cm$^2$ hr) for the same wall temperature range) and, unlike kerosene, did not show a velocity dependence, suggesting that deposit formation in natural gas may be limited by the kinetics of the deposition processes. Plating the inside of the copper tubes with nickel reduced deposit formation and eliminated tube corrosion in most cases. Similarly, in [35,36] the tests performed with natural gas have shown roughening and discoloration of the copper tube inner surface due to sulfidation. However, in [35,36] no significant carbon deposition was detected.

To better comprehend the corrosion phenomena found in the previous studies, an in depth study on the methane compatibility with copper and copper-based alloys were performed by US researchers [46,47]. Heated material specimens incorporating cooling channels were exposed to methane flow under realistic booster engine service conditions. To prevent material corrosion, specimens with electrodeposited gold and platinum coatings were also tested. Tests were conducted using either very pure grades of methane or methane doped with controlled contaminant. Metallurgical and chemical inspections of the specimens were than carried out. Such analyses indicated that there was no evidence of significant coke deposition and material corrosion in the channels up to 770 K of wall temperature when high purity methane was used. This result is also supported by the evidence that the heat transfer and the pressure drop measurements through the channel remained steady throughout each run. However, severe corrosion resulted when sulfur (in the form of methyl mercaptan, $CH_3SH$, or hydrogen sulfide, $H_2S$) was added to methane. Evidence of channel corrosion with the formation of cuprous sulfide ($Cu_2S$) was found. For sulfur levels as low as 10 ppm (by volume) of methyl mercaptan or 5 ppm (by volume) of $H_2S$ the build up of copper corrosion was severe enough to reduce the flow rate through the channel and thus degrade cooling channel performance substantially. The recommended specification for sulfur contaminant levels in methane intended for use in a reusable copper alloy thrust chamber is maximum 0.5 ppm (by volume). Finally, the effectiveness of protective coating materials was demonstrated with methane containing non-negligible trace amounts of sulfur compounds. This can be clearly noticed in Fig. 30.

To better reproduce the realistic heating occurring in rocket engine cooling channels, an experimental apparatus to investigate coolant decomposition and carbon deposition in a circular channel subjected to asymmetric heating was developed more recently by a further team of US researchers [49]. A copper or stainless steel channel was fitted between a heated copper block and an unheated support of refractory ceramic insulation. Cryogenic methane, pure or with added species (mainly: ethylene, $C_2H_4$, and propane, $C_3H_8$), was driven through the test section, with pressures that have exceeded 220 bar. The copper block was heated to temperatures up to 925 K. Analysis of the test section and of the effluent gas samples showed that, when at high temperature, methane with additive species thermally decomposes and forms heavier hydrocarbon compounds. Pure methane produces heavy hydrocarbons only at high temperatures and at a lower extent, and thus it can be considered a more thermally-stable coolant relative to methane-based fuels contaminated with minor hydrocarbon species.

In [50] the effect of sulfur impurities on methane flow in cooling channels was investigated by Japanese researchers. Minute amounts of hydrogen sulfide was mixed with methane at the upstream of the test section. The test section for sulfur attack was a circular tube made of a copper-based alloy and having an inner diameter of 2 mm. Methane was pre-heated in a heat exchanger prior to the test section and heated by an infrared radiation heater through the test section. Methane inlet pressure was up 30 bar and the wall temperature was up to 800 K. Both the flow resistance and the heat transfer were measured. The main outcome of this study was that the sulfur attack affects more the flow resistance rather than heat transfer performance. For instance, Fig. 31 shows that a concentration of 5 ppm of hydrogen sulfide did not affect the methane flow resistance and the heat transfer when the wall temperature was 600 K. On the other hand, when the wall temperature was increased to 800 K the flow resistance increased significantly while the heat transfer coefficient slightly increased.

## 5. Thrust chamber life

The thrust chambers have a limited life due to the plastic deformations that accumulate during engine operation. Typically, chamber life is defined as the number of firings before a partial rupture of the inner wall that separates the hot-gas from the coolant occurs. From the thermo-mechanical point of view, the pressure inside the cooling channel, that is higher than the pressure of the hot-gas, induces a bending of the inner wall separating the hot-gas from the coolant flow; furthermore, compressive hoop stresses arise in the inner wall since its

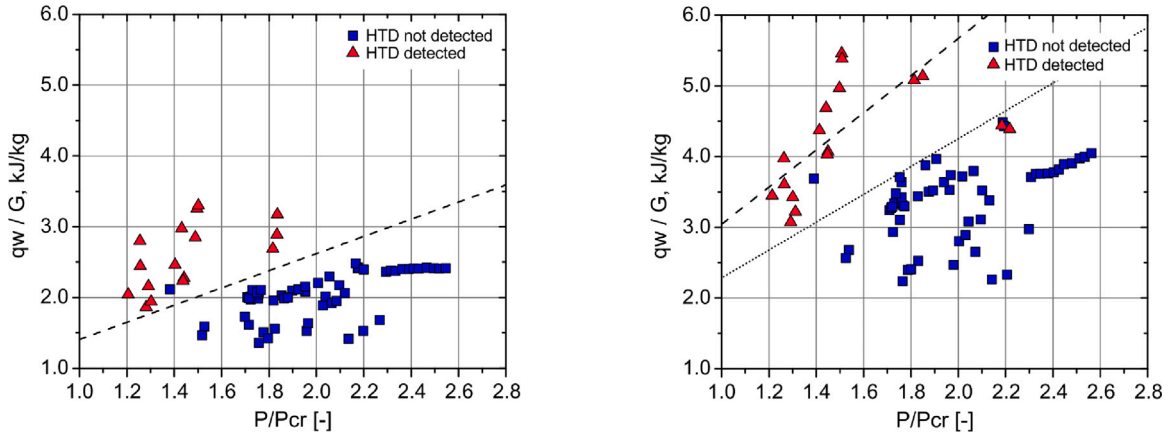


**Fig. 24.** Identification of methane heat transfer deterioration (HTD) for rectangular cooling channels with aspect ratio 1.67 (left) and 9.2 (right). On the x-axis: coolant pressure normalized with the methane critical pressure. On the y-axis: coolant heat-to-mass flux ratio in [kJ/kg]. Note: the heat flux is the hot-gas side heat flux averaged over the channel perimeter.
*Source:* (From [41]).

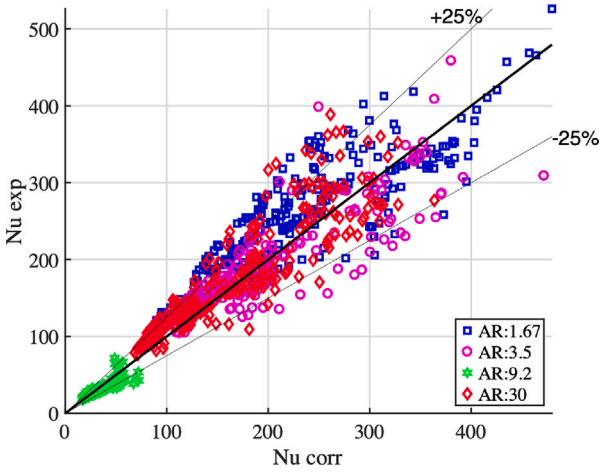


**Fig. 25.** Methane heat transfer data for rectangular cooling channels with different aspect ratios *AR*. On the x-axis: the computed Nusselt number using Eq. (7). On the y-axis: the experimental Nusselt number.
*Source:* (From [42]).

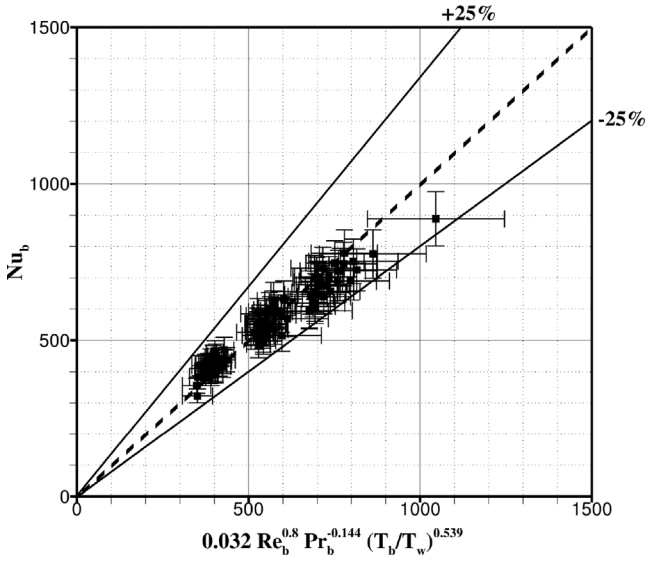


**Fig. 26.** Methane heat transfer data for rectangular cooling channels. On the x-axis: the computed Nusselt number using Eq. (8). On the y-axis: the experimental Nusselt number. Note that the data are plotted with the associated experimental error.
*Source:* (Data from [43]).

thermal expansion is restrained by the cold outer wall. The induced thermal stresses generally exceed the yield stress generating significant plastic deformations in the inner wall. Estimating the life of a chamber is a very complex thermo-mechanical problem which depends mainly on the heat transfer behavior, on the material properties in the visco-plastic regime, as well as on phenomena such as hot-gas side wall oxidation and coolant side wall corrosion. Among the typical thrust chamber failure mechanisms, creep, low-cycle fatigue, and ratcheting have been identified as the most likely causes of failure. Due to the complex interaction of these phenomena, which are often difficult to model, chamber life is typically demonstrated directly on real scale thrust chambers by accumulating multiple firings. However, some simplified and alternative approaches have been proposed in order to avoid direct testing of the final component, which is a complex and costly operation that occurs only when the design is in its final stage and is therefore difficult to revise heavily if needed. Such simplified approaches have been successfully applied by NASA in the 1970s in the case of oxygen–hydrogen propulsion [51,52] and, more recently, by DLR using liquid nitrogen as surrogate coolant and laser heating as surrogate hot-gas convection [53] and by TUM in the case of oxygen–methane propulsion [54,55]. In particular, the experimental apparatus put in place by TUM was comprised of an actively cooled fatigue specimen which was mounted downstream of a sub scale combustion chamber with a rectangular cross-section and fed with gaseous oxygen and gaseous methane ejected from 5 in a row coaxial injection elements. The test section, mounted upstream of the nozzle, housed a replaceable fatigue specimen with 17 rectangular cooling channels that were fed with supercritical-pressure nitrogen at ambient temperature. The cooling channels had a height of 8 mm, a width of 2.5 mm, a rib thickness of 2 mm, an inner wall thickness of 1 mm, and a length of 96 mm. The fatigue specimen, made of a copper-based alloy, was loaded cyclically and inspected by a laser profile scanner after each cycle. Furthermore, the specimen was equipped with a set of thermocouples in different positions and depths to measure the temperature distribution in the structure during each cycle. Chamber pressure was about 17 bar which was held for 20 s. The nitrogen inlet pressure in each test was regulated to 70 bar. During the tests the cooling channel mass flow rate was decreased, until the desired wall temperature level was reached, for which plastic deformations has been expected. After that, several tests

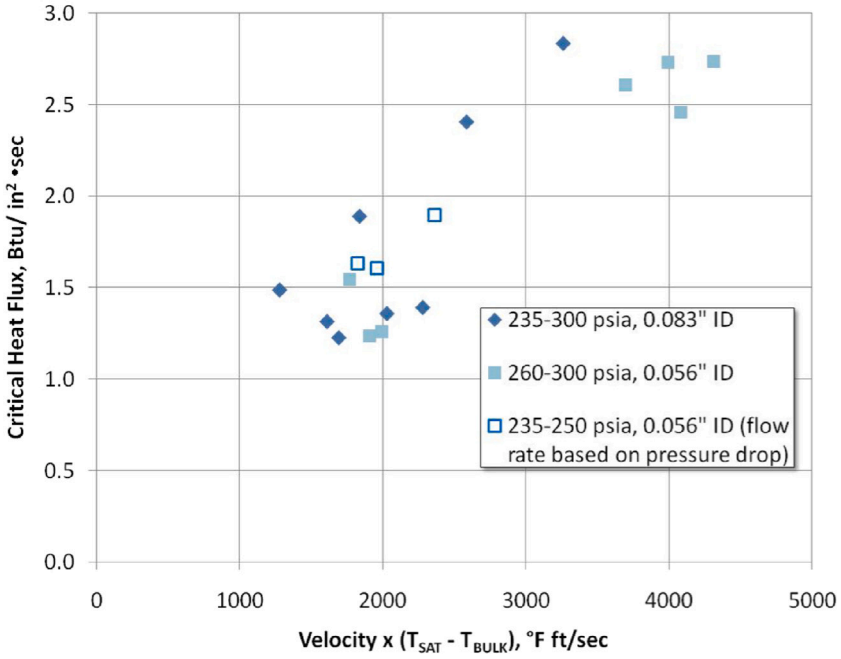


**Fig. 27.** Methane critical heat flux data for circular tubes with different diameters and for pressures from 16 to 21 bar. On the x-axis: the product of the flow velocity and subcooling, i.e., $u\left(T_{sat}-T_b\right)$ in [°F ft/s]. On the y-axis: the critical heat flux in [BTU/(in$^2$ s)].
*Source:* (From [44]).

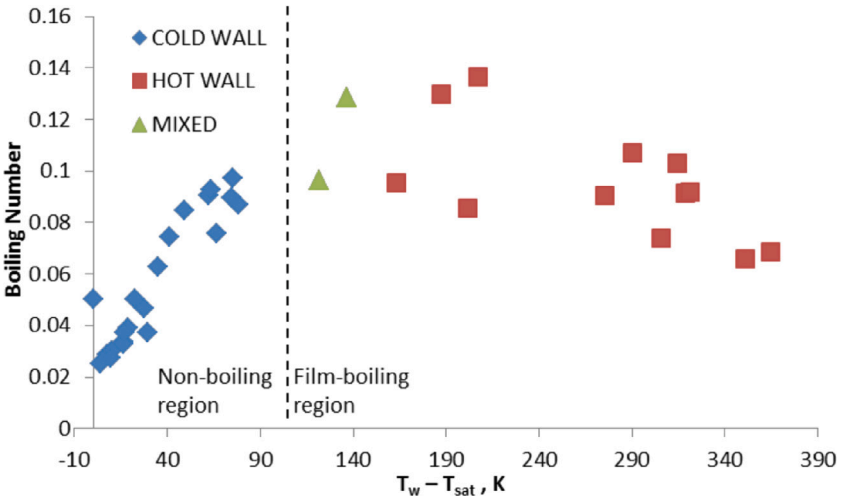


**Fig. 28.** Boiling number for the methane flow in a rectangular channel having a cross-section of 1.8 mm × 4.1 mm (base × height). On the x-axis: the average wall temperature minus saturation temperature, $T_w - T_{sat}$ in [K]. On the y-axis: the Boiling number.
*Source:* (From [45]).

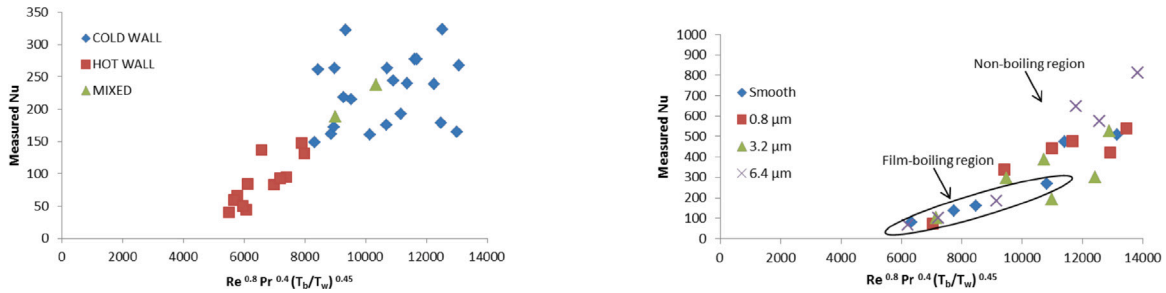


**Fig. 29.** Methane heat transfer data for rectangular and square cooling channels. Left: results for the rectangular channel having a cross-section of 1.8 mm × 4.1 mm (base × height). Right: results for the square channels with a cross-section of 3.2 mm × 3.2 mm and different surface finishes. On the x-axis: the number $Re_b^{0.8}Pr_b^{0.4}\left(\frac{T_b}{T_w}\right)^{0.45}$. On the y-axis: the experimental Nusselt number.
*Source:* (From [45]).

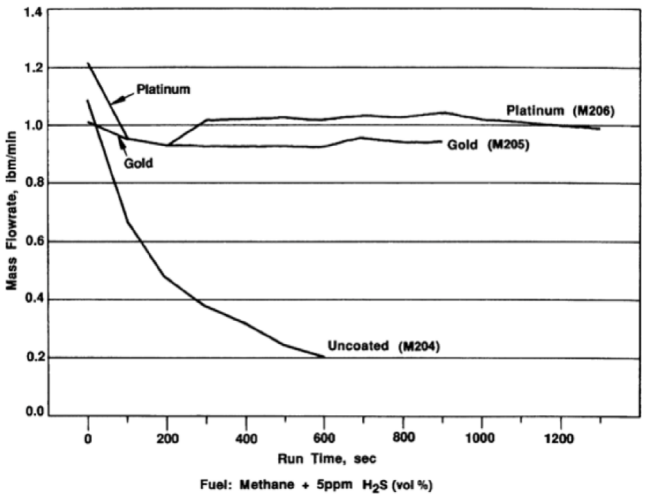


**Fig. 30.** Effect of sulfur contamination (5 ppm of hydrogen sulfide by volume) on coolant mass flow rate over the test run time for uncoated and coated (gold and platinum) copper cooling channels. On the x-axis: test run time in [s]. On the y-axis: coolant mass flow rate in [$lb_m$/min].
*Source:* (From [48]).

with the identified cooling channel mass flow rate were conducted. An increasing plastic deformation during the test campaign was measured. In [54], with an operative set-up that led to a maximum hot-gas side wall temperature of about 930 K, after 45 load cycles the inner cooling channel surface bulged 0.8 mm outward in the direction to the hot-gas and the wall thickness between hot-gas and coolant decreased from initial 1.0 mm to about 0.6 mm (Fig. 32).

In [55], using the same apparatus, a fatigue specimen was loaded cyclically until its failure, that occurred after the 48 cycle. Chamber pressure was about 19 bar and the maximum hot-gas side wall temperature was about 1000 K. The experimental results have shown that the average roughness *Ra* of the hot-gas side surface was increased nearly linearly with the number of load cycles. Fig. 33 shows that, when the incremental thinning of the wall exposed to the hot-gas led to a critical value, the wall eventually fails. Such failure is characterized by a deformation of the cooling channel cross-section in a "doghouse-like" shape. It is recognized in [55] that the yielding, mostly caused by tensile stresses during the combustion shut-down phase, is the dominant life-limiting effect. This phenomenon is accelerated by the surface roughness increase by chemical oxidation–reduction of the surface in contact with the combustion gas (i.e., blanching effect), which increases the wall heat flux and thereby the thermal loading. Moreover, it is recognized that the effect of material creep-relaxation is presumably small, due to the short total duration of heat load.

## 6. Conclusions

The recent interest in oxygen–methane rocket propulsion has underlined the need to carefully review the experimental studies pertinent to the heat transfer behavior inside the thrust chambers. These studies, which date back to the end of the 70 s, allow the following main conclusions to be drawn:

- The hot-gas side heat transfer correlates similarly to the case of oxygen–hydrogen and oxygen–kerosene. Still compared to these propellants, there is a qualitatively similar behavior as regards the increase of the heat transfer with the combustion chamber pressure and the mixture ratio approaching the stoichiometric value. However, the effect of the mixture ratio in the region near the injector is not clear.
- In the region near the injector, the heat transfer to the chamber wall is impacted by the injector element configuration. Experiments indicate that swirl coaxial elements promote higher heat flux than shear coaxial elements. Furthermore, increasing the recess of the oxygen post or the fuel-to-oxidizer momentum flux ratio increases the heat transfer. These results are qualitatively similar to those found with other propellant combinations such as oxygen–hydrogen.
- Effective means to reduce the hot-gas side heat transfer are: mixture ratio bias, film cooling, and surface coating. Although much depends on the mass flow rates used, mixture ratio bias is found to be more effective than film cooling because it is able to cool a greater length of the chamber. As for the hot-gas side surface coating, both zirconia and nickel coatings were tested. Success was only partial as cracks developed as firing time accumulated. However, the nickel plating appeared to be more promising.
- Significant reduction of hot-gas side heat transfer caused by carbon deposition is not detected.
- The hot-gas side heat transfer in additively manufactured thrust chambers is substantially greater than in conventional thrust chambers, although the hot-gas flow induces a smoothing of the surface which is beneficial in partially reducing the heat transfer.
- Coolant heat transfer when using supercritical methane flowing in heated tubes with circular cross-section behaves similarly to other single-phase fluids. In fact, data fairly correlate with Dittus-Boelter type equations and the heat transfer coefficient decreases when increasing the wall temperature. In addition, as expected, the heat transfer coefficient increases with increasing surface roughness.
- Heat transfer deterioration in cooling channels may occur in case of supercritical methane. However, a certain level of surface roughness or operative pressure sufficiently far from the critical value prevent the onset of this phenomenon.
- Critical heat flux of subcritical methane in cooling channels increases, as expected, with increasing flow velocity and fluid subcooling.
- Methane heat transfer in rectangular cooling channels with asymmetric heating can be still correlated using Dittus-Boelter type equations although the three-dimensional nature of the problem poses serious limits on the validity of such an approach.
- Severe corrosion of the cooling channel walls occurs when even small parts, in the order of parts per million, of sulfur compounds are present in the methane. On the other hand, carbon deposition on the channel walls is almost absent, especially in case of pure methane.
- Thermo-mechanical life of thrust chambers can be studied with simplified apparatuses, provided that these contain the main elements that characterize the real thrust chambers, such as the chemically aggressive environment of the hot-gas, channels with rectangular section and representative temperature and heat flux levels.

Despite the many studies done so far and the significant outcomes on the heat transfer relevant to oxygen–methane thrust chambers, some aspects still remain poorly understood or little investigated. Aspects that would need further insight are:

- *The hot-gas side heat transfer in the region near the injection*. The heat transfer in the flame formation zone depends on multiple factors that need to be further investigated, such as, for example, the type and geometry of the injection elements, the mixture and the momentum ratio of the propellants, the distance between the injection elements, and the distance between the injection elements and the chamber wall. Furthermore, the heat transfer

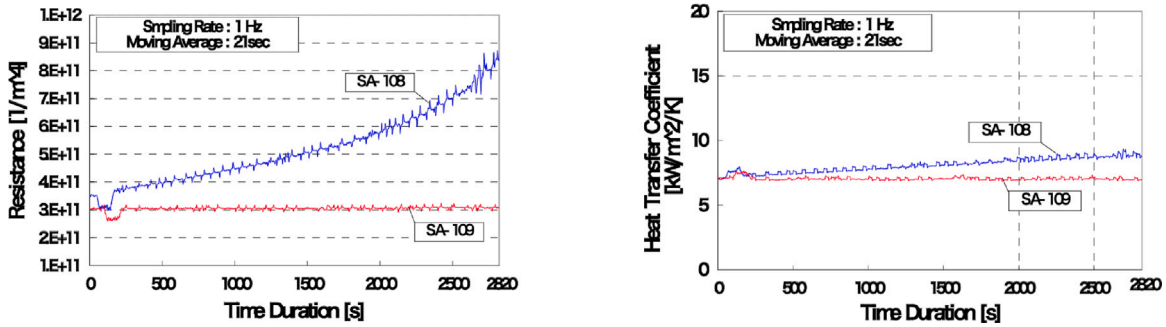


**Fig. 31.** Effect of sulfur contamination (5 ppm of hydrogen sulfide) on coolant flow resistance (left) and heat transfer coefficient (right) over the test run time for a wall temperature of 600 K (red line) and 800 K (blue line). On the x-axis: test run time in [s]. On the y-axis: the flow resistance $\rho\Delta p/\dot{m}^2$ in $[1/m^4]$ (left) and the heat transfer coefficient in $[kW/(m^2\ K)]$ (right). (For interpretation of the references to color in this figure legend, the reader is referred to the web version of this article.)
*Source:* (From [50])

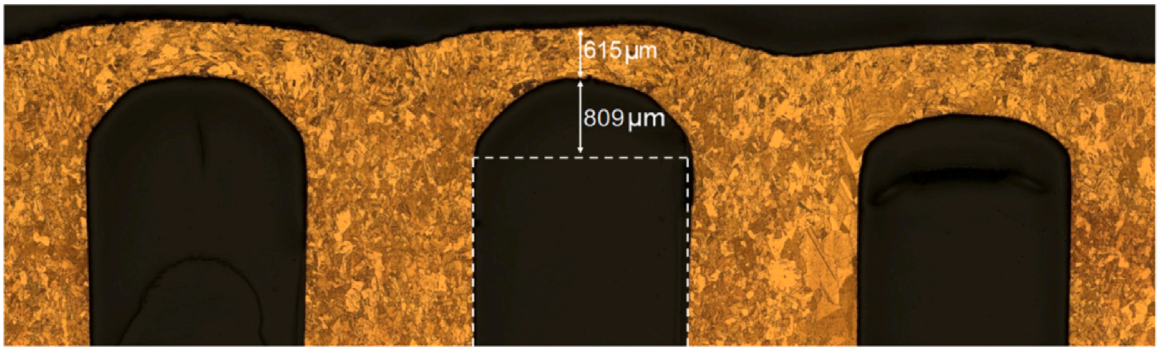


**Fig. 32.** Fatigue specimen's cut view after 45 load cycles.
*Source:* (From [54]).

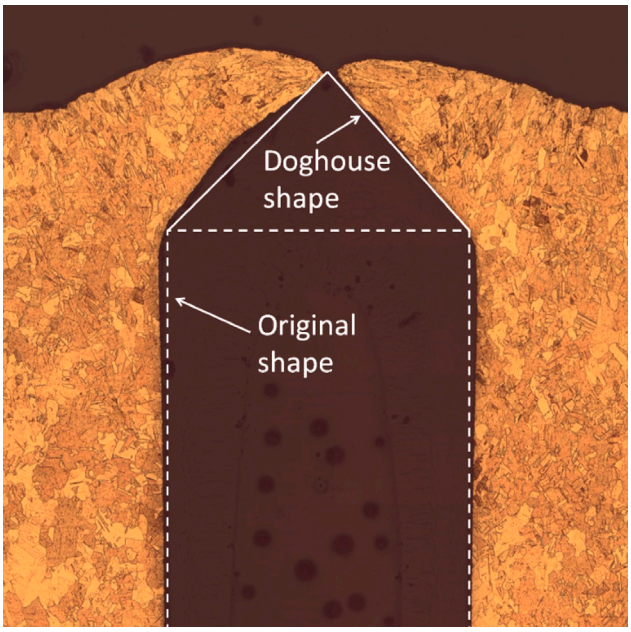


**Fig. 33.** Fatigue specimen's cut view after 48 load cycles; detail of the failed region.
*Source:* (From [55]).

to the injector faceplate, also due to its difficult instrumentation, is still completely unexplored.

- *Methods to reduce the hot-gas side heat transfer*. Although methods such as film cooling, mixing ratio bias, and surface coating have been investigated, systematic studies for the specific case of oxygen–methane propulsion are still lacking. It is important to note that the need to reduce the hot-gas side heat transfer may decade in specific applications where an increase in heat transfer is desired, such as in expander-cycle engines.
- *Methane heat transfer in real cooling channels*. While straight channels with circular cross-section and homogeneous heating have been extensively used in the experiments having provided fairly consolidated and coherent data, the heat transfer in realistic cooling channels is not yet fully characterized. In fact, since real cooling channels are characterized by asymmetric heating, rectangular cross-section, and possibly curvature, specific studies should be promoted.
- *The effect and the potentiality of the additive manufacturing on the coolant side heat transfer*. Additive manufacturing offers great opportunities to rethink the design of cooling channels, which could include non-rectangular cross-sections, internal ribs, non-conventional materials, etc. However, the introduction of unconventional designs must be accompanied by adequate studies on the heat transfer. In addition, the use of additive manufacturing requires an in-depth study of the effect of surface roughness, as it is much greater than that typical of conventional manufacturing.
- *Coolant heat transfer for methane at subcritical pressure*. The heat transfer of subcritical methane, i.e. in case of two-phase flow, has only occasionally been studied. Further studies are required in order to better characterize the heat transfer coefficient and especially the critical heat flux. However, it should be noted that these studies are of interest only in the case of pressure-fed

thrust chambers or possibly in the case of pump-fed thrust chambers during the transient phases of engine startup and shutdown or during throttled engine operation, as required, for example, during the landing phase of reusable systems.

- *Characterization of the thrust chamber life*. While it has been demonstrated that chamber life can be analyzed with simplified experimental setups, a comprehensive characterization of this problem is still lacking. For instance, it should be understood in more detail how the life of the chambers depends on the maximum wall temperature, on the thermo-mechanical properties of the material, especially in the case of additive manufacturing, on the thickness of the inner and outer walls, on the roughness of the surfaces, on the transient phases during engine ignition and shut-down, on the hot-fire duration, and on the propellant mixture ratio.

These conclusions, which highlight the main established results and aspects that require further investigation, may be of interest to rocket engine designers and help plan future research and development activities related to oxygen–methane propulsion.

## Declaration of competing interest

The authors declare that they have no known competing financial interests or personal relationships that could have appeared to influence the work reported in this paper.

## References


[1] G.P. Sutton, O. Biblarz, Rocket Propulsion Elements, seventh ed., John Wiley & Sons, INC., 2001.

[2] E. Armstrong, J. Schlumberger, Cooling of rocket thrust chambers with liquid oxygen, AIAA Paper 90-2120, 1990, http://dx.doi.org/10.2514/6.1990-2120.

[3] F. Kerstens, A. Cervone, P. Gradl, End to end process evaluation for additively manufactured liquid rocket engine thrust chambers, Acta Astronaut. 182 (2021) 454–465, http://dx.doi.org/10.1016/j.actaastro.2021.02.034.

[4] C.R. Bailey, Oxygen/hydrocarbon combustion device technology, in: Proceedings of 1985 JANNAF Propulsion Meeting, Vol. 1, Chemical Propulsion Information Agency, CPIA, 1985, pp. 271–280.

[5] C.R. Bailey, RP-1 and methane combustion and cooling experiments, in: Advanced Earth-To-Orbit Propulsion Technology 1986, Vol. 2, National Aeronautics and Space Administration, NASA, 1986, pp. 529–548.

[6] H.P. Trinh, Liquid methane/oxygen injector study for potential future mars ascent engines, AIAA Paper 2000-3119, 2000, http://dx.doi.org/10.2514/6.2000-3119.

[7] J. Melcher, J. Allred, Liquid oxygen/liquid methane test results of the RS-18 lunar ascent engine at simulated altitude conditions at NASA white sands test facility, AIAA Paper 2009-4949, 2009, http://dx.doi.org/10.2514/6.2009-4949.

[8] T. Smith, M. Klem, K. Fisher, Propulsion risk reduction activities for non-toxic cryogenic propulsion, AIAA Paper 2010-8680, 2010, http://dx.doi.org/10.2514/6.2010-8680.

[9] T. Brown, M. Klem, P. McRight, Foundational methane propulsion related technology efforts, and challenges for applications to human exploration beyond earth orbit, in: Proceedings of Space Propulsion Conference 2016, 2016, pp. 1–12.

[10] N. Zhang, W.-B. Wang, J.-G. Sun, Demonstration of a 600 kn class LOX/methane rocket engine, in: Proceedings of 63$^{Rd}$ International Astronautical Congress, 2012, pp. 1–4.

[11] H. Asakawa, H. Nanri, K. Aoki, I. Kubota, H. Mori, Y. Ishikawa, K. Kimoto, S. Ishihara, S. Ishizaki, The status of the research and development of LNG rocket engines in Japan, in: L.T. De Luca, T. Shimada, V.P. Sinditskii, M. Calabro (Eds.), Chemical Rocket Propulsion - a Comprehensive Survey of Energetic Materials, Springer International Publishing, 2017, pp. 463–487.

[12] J.-P. Dutheil, Y. Boué, Highly reusable LOX/LCH$_4$ ACE rocket engine designed for SpacePlane: technical maturation progress via key system demonstrators results, in: Proceedings of 7th European Conference for Aeronautics and Space Sciences, EUCASS, 2017, pp. 1–15.

[13] M. Harris, The heavy lift: Blue origin's next rocket engine could power our return to the moon, IEEE Spectr. 56 (7) (2019) 26–30, http://dx.doi.org/10.1109/MSPEC.2019.8747308.

[14] P. Simontacchi, E. Edeline, R. Blasi, S. Sagnier, A. Remy, A. Espinosa-Ramos, PROMETHEUS: precursor of a new low-cost rocket engine family, in: Proceedings of Space Propulsion Conference 2020, 2021, pp. 1–6.

[15] T. Traudt, M. Börner, D. Suslov, R.d.S. Hahn, A.M. Saraf, J. Deeken, J. Hardi, S. Schlechtriem, Liquid upper stage demonstrator engine (LUMEN): component test results and project progress, in: Proceedings of Space Propulsion Conference 2022, 2022, pp. 1–9.

[16] F. Battista, D. Ricci, P. Natale, D. Cardillo, M. Fragiacomo, S. Franchitti, M. Ferraiuolo, V. Salvatore, Recent achievements regarding the research activities on hyprob LOX/CH$_4$ demonstrators line, in: Proceedings of Space Propulsion Conference 2022, 2022, pp. 1–11.

[17] D. Kajon, C. Boffa, P. Vinet, D. Liuzzi, M. Rudnykh, G. Caggiano, D. Drigo, D. Schiariti, F. Di Matteo, N. Ierardo, A. Paragina Sirbi, Development of the liquid oxygen and methane M10 rocket engine for the Vega-E upper stage, in: Proceedings of Space Propulsion Conference 2022, 2022, pp. 1–7.

[18] A. Kumakawa, M. Sasaki, K. Sato, H. Tamura, F. Ono, H. Sakamoto, N. Yatsuyanagi, Hot gas side heat transfer characteristics of LOX/H$_2$ and LOX/HC type propellants, report NAL-TR-1062T, Japan Aerospace Exploration Agency, JAXA, 1990.

[19] G.M. Meagher, J.A. Muss, Swirl coaxial injector element characterization for booster engines, in: Advanced Earth-to-Orbit Propulsion Technology 1988, Vol. 1, National Aeronautics and Space Administration, NASA, 1988, pp. 334–347.

[20] R.J. Jensen, H.C. Dodson, S.E. Claflin, LOX/hydrocarbon combustion instability investigation, report NASA-CR-182249, National Aeronautics and Space Administration, NASA, 1989, contract NAS3-24612.

[21] J. Volkmann, L. Tuegel, J. McLeod, Gas side heat flux and film coolant investigation for advanced LOX/hydrocarbon thrust chambers, AIAA Paper 90-2184, 1990, http://dx.doi.org/10.2514/6.1990-2184.

[22] H. Tamura, F. Ono, A. Kumakawa, N. Yatsuyanagi, LOX/methane staged combustion rocket combustor investigation, AIAA Paper 87-1856, 1987, http://dx.doi.org/10.2514/6.1987-1856.

[23] A. Kumakawa, M. Sasaki, K. Sato, F. Ono, H. Sakamoto, N. Vatsuyanagi, Characteristics of heat transfer to nickel plated chamber walls of high pressure rocket combustors, report NAL-TR-1126T, Japan Aerospace Exploration Agency, JAXA, 1991.

[24] S. Ukai, K. Sakaki, Y. Ishikawa, H. Sakaguchi, S. Ishihara, Component tests of a LOX/methane full-expander cycle rocket engine: injector and regeneratively cooled combustion chamber, in: Proceedings of 8th European Conference for Aeronautics and Space Sciences, EUCASS, 2019, pp. 1–9.

[25] R. Arnold, D.I. Suslov, O.J. Haidn, Experimental investigation of film cooling with tangential slot injection in a LOX/CH$_4$ subscale rocket combustion chamber, in: Transactions of the Japan Society for Aeronautical and Space Sciences, Space Technology Japan, 7 (ists26), The Japan society for aeronautical and space sciences, 2009, pp. 81–86.

[26] D. Suslov, J. Haemisch, J. Hardi, M. Oschwald, Selective laser manufactured copper alloy nozzle for a subscale thrust chamber, in: Proceedings of Space Propulsion Conference 2020, 2021, pp. 1–6.

[27] M. Pizzarelli, Overview and analysis of the experimentally measured throat heat transfer in liquid rocket engine thrust chambers, Acta Astronaut. 184 (2021) 46–58, http://dx.doi.org/10.1016/j.actaastro.2021.03.028.

[28] O. Haidn, M.P. Celano, L. Meng, R. Christof, S. Silvestri, N. Slavinskaya, On methane/oxygen combustion for rocket applications, in: Proceedings of the International Symposium on Innovation and Prospects of Liquid Propulsion Technology, 2016, pp. 1–10.

[29] M.P. Celano, S. Silvestri, G. Schlieben, C. Kirchberger, O.J. Haidn, T. Dawson, R. Ranjan, S. Menon, Numerical and experimental investigation for a GOX-gCH$_4$ shear-coaxial injector element, in: Proceedings of Space Propulsion Conference 2014, 2014, pp. 1–13.

[30] S. Silvestri, M.P. Celano, G. Schlieben, O.J. Haidn, Characterization of a multi-injector GOX-gCH$_4$ combustion chamber, AIAA Paper 2016-4992, 2016, http://dx.doi.org/10.2514/6.2016-4992.

[31] S. Silvestri, M.P. Celano, C. Kirchberger, G. Schlieben, O. Haidn, O. Knab, Investigation on recess variation of a shear coax injector for a single element GOX-gCH$_4$ combustion chamber, in: Transactions of the Japan Society for Aeronautical and Space Sciences, Aerospace Technology Japan, 14 (ists30), The Japan society for aeronautical and space sciences, 2016, pp. 13–20.

[32] J.M. Locke, S. Pal, R.D. Woodward, Chamber wall heat flux measurements for a LOX/CH$_4$ uni-element rocket, AIAA Paper 2007-5547, 2007, http://dx.doi.org/10.2514/6.2007-5547.

[33] L. Vingert, P. Grenard, F. Lévy, A. Nicole, L.H. Dorey, M.M. Benito, Heat transfer measurements in a water-cooled rocket combustion chamber operated with oxygen/methane mixtures at the mascotte test facility, in: Proceedings of 32nd ISTS & 9th NSAT Joint Symposium, 1-7, 2019, pp. 1–9.

[34] A.J. Giovanetti, L.J. Spadaccini, E.J. Szetela, Deposit formation and heat transfer in hydrocarbon rocket fuels, report NASA-CR-168277, National Aeronautics and Space Administration, NASA, 1983, contract NAS3-23344.

[35] R.T. Cook, Methane heat transfer investigation. 8th bi-monthly technical progress narrative. Period of performance: 14 april - 14 june 1984, report NASA-CR-171051, National Aeronautics and Space Administration, NASA, 1984, contract NAS8-34977.

[36] R.T. Cook, Methane heat transfer investigation. Technical progress narrative. Period of performance: 15 August thru October 31, report NASA-CR-171199, National Aeronautics and Space Administration, NASA, 1984, contract NAS8-34977.

[37] S.E. Claflin, J.C. Volkmann, Material compatibility and fuel cooling limit investigation for advanced LOX/hydrocarbon thrust chambers, AIAA Paper 90-2185, 1990, http://dx.doi.org/10.2514/6.1990-2185.

[38] K. Liang, B. Yang, Z. Zhang, Investigation of heat transfer and coking characteristics of hydrocarbon fuels, J. Propuls. Power 14 (5) (1998) 789–796, http://dx.doi.org/10.2514/2.5342.

[39] H. Gu, H. Li, H. Wang, Y. Luo, Experimental investigation on convective heat transfer from a horizontal miniature tube to methane at supercritical pressures, Appl. Therm. Eng. 58 (1–2) (2013) 490–498, http://dx.doi.org/10.1016/j.applthermaleng.2013.04.049.

[40] T. Kato, D. Terakado, H. Nanri, T. Morito, I. Masuda, H. Asakawa, H. Sakaguchi, Y. Ishikawa, T. Inoue, S. Ishihara, M. Sasaki, Subscale firing test for regenerative cooling LOX/methane rocket engine, in: Proceedings of 7th European Conference for Aeronautics and Space Sciences, EUCASS, 2017, pp. 1–12.

[41] J. Haemisch, D. Suslov, M. Oschwald, Experimental study of methane heat transfer deterioration in a subscale combustion chamber, J. Propuls. Power 35 (4) (2019) 819–826, http://dx.doi.org/10.2514/1.B37394.

[42] J. Haemisch, D. Suslov, M. Oschwald, Experimental investigations of heat transfer processes in cooling channels for cryogenic hydrogen and methane at supercritical pressure, in: F. Di Mare, A. Spinelli, M. Pini (Eds.), Non-Ideal Compressible Fluid Dynamics for Propulsion and Power, Springer Cham, 2020, pp. 3–16.

[43] R. Votta, F. Battista, V. Salvatore, M. Pizzarelli, G. Leccese, F. Nasuti, S. Meyer, Experimental investigation of transcritical methane flow in rocket engine cooling channel, Appl. Therm. Eng. 101 (2016) 61–71, http://dx.doi.org/10.1016/j.applthermaleng.2015.12.019.

[44] J. Van Noord, A heat transfer investigation of liquid and two-phase methane, report NASA-TM—2010-216918, National Aeronautics and Space Administration, NASA, 2010.

[45] A. Trejo, A. Trujillo, M. Galvan, A. Choudhuri, J.C. Melcher, J.J. Bruggemann, Experimental investigation of methane convection and boiling in rocket engine cooling channels, J. Thermophys. Heat Transfer 30 (4) (2016) 937–945, http://dx.doi.org/10.2514/1.T4883.

[46] S.D. Rosenberg, M.L. Gage, Compatibility of hydrocarbon fuels with booster engine combustion chamber liners, J. Propuls. Power 7 (6) (1991) 922–928, http://dx.doi.org/10.2514/3.23410.

[47] S.D. Rosenberg, M.L. Gage, G.D. Homer, J.E. Franklin, Hydrocarbon-fuel/copper combustion chamber liner compatibility, corrosion prevention, and refurbishment, J. Propuls. Power 8 (6) (1992) 1200–1207, http://dx.doi.org/10.2514/3.11462.

[48] M.L. Gage, S.D. Rosenberg, Hydrocarbon fuel/combustion-chamber liner materials compatibility. interim final report, report NASA-CR-185203, National Aeronautics and Space Administration, NASA, 1990, contract NAS3-25070.

[49] R. Driscoll, T. Moore, B.B. Brady, S. Frolik, J.H. Morehart, Carbon deposit formation in supercritical methane-based, hydrocarbon fuels using a cooling channel surrogate, AIAA Paper 2019-3939, 2019, http://dx.doi.org/10.2514/6.2019-3939.

[50] N. Azuma, M. Sato, M. Tadano, M. Sato, T. Masuoka, S. Moriya, K. Aoki, H. Kawashima, M. Yoshida, K. Okita, T. Tamura, K. Niu, Compatibility of methane fuel with LOX/methane engine combustion chamber cooling channels, AIAA Paper 2008-4838, 2008, http://dx.doi.org/10.2514/6.2008-4838.

[51] R.J. Quentmeyer, Experimental fatigue life investigation of cylindrical thrust chambers, AIAA Paper 77-893, 1977, http://dx.doi.org/10.2514/6.1977-893.

[52] N.P. Hannum, H.J. Kasper, A.J. Pavli, Experimental and theoretical investigation of fatigue life in reusable rocket thrust chambers, AIAA Paper 76-685, 1976, http://dx.doi.org/10.2514/6.1976-685.

[53] J.R. Riccius R.G. Thiede, S. Reese, Life prediction of rocket combustion-chamber-type thermomechanical fatigue panels, J. Propuls. Power 33 (6) (2017) 1529–1542, http://dx.doi.org/10.2514/1.B36361.

[54] F. Hötte, T. Fiedler, M.C. Haupt, P. Lungu, C.V. Sethe, O.J. Haidn, Experimental investigations of thermomechanical fluid–structure interaction in rocket combustion chambers, J. Propuls. Power 35 (5) (2019) 906–916, http://dx.doi.org/10.2514/1.B37439.

[55] F. Hötte, C.V. Sethe, T. Fiedler, M.C. Haupt, O.J. Haidn, M. Rohdenburga, Experimental lifetime study of regeneratively cooled rocket chamber walls, Int. J. Fatigue 138 (2020) 1–12, http://dx.doi.org/10.1016/j.ijfatigue.2020.105649, Paper number 105649.